The sorption and diffusion of ^{133}Ba in granitic rocks

Master's thesis

University of Helsinki
Faculty of Science
Department of Chemistry
Laboratory of Radiochemistry

Eveliina Muuri

13.11.2015

HELSINGIN YLIOPISTO – HELSINGFORS UNIVERSITET – UNIVERSITY OF HELSINKI

Tiedekunta/Osasto Fakultet/Sektion – Faculty Faculty of Science	Laitos/Institution– Department Department of Chemistry	
Tekijä/Författare – Author Eveliina Marianne Muuri		
Työn nimi / Arbetets titel – Title The sorption and diffusion of ^{133}Ba in granitic rocks		
Oppiaine /Läroämne – Subject Radiochemistry		
Työn laji/Arbetets art – Level Master's thesis	Aika/Datum – Month and year 11/2015	Sivumäärä/ Sidoantal – Number of pages 76

Tiivistelmä/Referat – Abstract

The distribution coefficients of barium in the Olkiluoto pegmatite, veined gneiss, Grimsel granodiorite and their main minerals (quartz, plagioclase, potassium feldspar and biotite) were obtained by batch sorption experiments carried out as a function of the concentration of barium. The distribution coefficients were modelled with the PHREEQC calculation code. The results of different rocks and minerals were compared with each other and the sorption mechanisms onto different mineral surfaces were evaluated. The sorption results of barium were also compared with sorption results obtained from a previous study for caesium. In addition, the diffusion of barium into the rock cubes was also studied both experimentally and computationally. Furthermore, the rock cubes from the diffusion experiments were studied with autoradiography and scanning electron microscopy.

The results showed that the distribution coefficients of barium were largest on biotite and the sorption as a function of the concentration of barium on all the minerals followed the same trend. The distribution coefficient results of veined gneiss, pegmatite and granodiorite followed the results of their main minerals. The distribution coefficients were largest on granodiorite which suggests ion exchange between barium and calcium, which is a common element in plagioclase occurring abundantly in granitic rock. It was also discovered that the distribution coefficients in saline water were considerably smaller than the results obtained from previous studies in low salinity water. This suggests that competing ions play a significant role in the sorption of barium.

Finally, the concentration decrease of barium in the diffusion experiments was largest in granodiorite which can be explained with both the porous structure of all the minerals of granodiorite and with the sorption properties of barium. It was discovered with autoradiography that the barium was mainly sorbed in the dark minerals of the rocks, but, additionally, barium sorption on plagioclase was also concluded to be significant. In addition, the sorbed barium could be seen with scanning electron microscopy on the biotite veins in the fracture zones of the rock confirming that the barium was sorbed.

Avainsanat – Nyckelord – Keywords

Barium, deep geological repository, sorption, diffusion, PHREEQC, Comsol, FE-SEM

Säilytyspaikka – Förvaringställe – Where deposited

Kumpulan kampuskirjasto, Helsingin yliopiston kirjallinen arkisto, E-thesis

Muita tietoja – Övriga uppgifter – Additional information

Contents

1. Introduction

The final disposal of nuclear fuel in Finland will be performed deep into the crystalline granitic bedrock in the Olkiluoto site. The repository system is based on a multiple barrier system consisting of copper-iron canisters isolated by bentonite and the bedrock. Furthermore, the underground openings will additionally be plugged with concrete [Miller and Marcos, 2007]. The bedrock in the Olkiluoto site is suitable for the disposal because of its stable tectonic situation, its good quality, existing reducing conditions and low groundwater flow in the depths of the repository system [Posiva Oy, 2012]. Due to the multiple release barriers, the final disposal of nuclear fuel is generally considered safe. However, there are several processes affecting the migration of the radionuclides from the nuclear fuel that need to be taken into account when assessing the safety of the repository. It is thus crucial to investigate the sorption and diffusion of radionuclides both through laboratory and in-situ field work to thoroughly assess the physical and chemical processes affecting the migration of radionuclides in the different release barriers, such as bentonite and bedrock.

The radionuclides in the nuclear fuel have been divided into five priority classes, the first of which is the top priority class containing the non-sorbing radionuclides which are expected to dominate the radioactive dose from the nuclear fuel (^{14}C, ^{36}Cl, ^{129}I). ^{226}Ra is placed in the low priority class but it is needed to be taken into account in some calculation cases in the biosphere assessment [Posiva, 2009]. However, the investigation of ^{226}Ra is complicated due to its being an alpha emitter and a part of the uranium series and it is therefore common to use the gamma emitting ^{133}Ba as an analogue for ^{226}Ra.

Differing from the Finnish safety calculation, it has been noted in some scenarios of the safety assessments that one of the largest long-term radiological risks to humans over a certain time span will be caused by radium [Hedin, H. et al, 2013]. The compounds of radium are relatively soluble which makes it mobile should a leakage occur. Barium and radium are both alkali earth metals with similar chemical properties and, furthermore, barium has been used as an analogue for radium and ^{133}Ba is one of the nuclides studied in the in-situ experiments [Widestrand, H. et al., 2004].

The sorption and diffusion of barium have been studied extensively in laboratory and in-situ conditions [Möri et. al, 2003; Hakanen, M. et al., 2012]. However, long-term in-situ experiments are very costly and time-consuming and, consequently, only few of them have been carried out. In 2009 a long-term diffusion project in the rock laboratory of the Grimsel test site in Switzerland was started to evaluate the matrix diffusion and sorption properties of radionuclides in in-situ conditions [Jokelainen et. al, 2012; Soler, J.M. et al., 2015; Ikonen, J. et al., 2015]. Additionally, several in-situ diffusion tests are ongoing in the Olkiluoto site [Voutilainen, M. et al., 2014]. These experiments need supporting laboratory studies as well as pre- and post-mortem modelling. It is thus highly important to evaluate the results from the laboratory experiments compared with the scarce in-situ results to better assess the relevance of the laboratory experiments.

The aim of this study was to investigate the sorption and diffusion of ^{133}Ba with laboratory experiments and with computer modelling to support the results from the in-situ experiments. The laboratory experiments were conducted in conditions resembling the Olkiluoto and Grimsel in-situ conditions. The sorption was studied with batch sorption experiments in a broad concentration range (10^{-9} – 10^{-3} M) in Grimsel granodiorite, Olkiluoto pegmatite and veined gneiss, and their main minerals; quartz, plagioclase, potassium feldspar and biotite. Diffusion, on the other hand, was studied in rock cubes of granodiorite, pegmatite and veined gneiss as a function of time. Groundwater simulants resembling the fracture waters in the Grimsel and Olkiluoto sites were used. In addition, all experiments were conducted at room temperature in oxic conditions.

Both the sorption and diffusion results were modelled with the PHREEQC computer program. In addition, COMSOL software was employed in the modelling of the diffusion results. The aim of the modelling was to combine the sorption and diffusion models in order to get closer to a reactive transport modelling which describes the retention of radionuclides in the geosphere in the conditions of the geological repository better.

2. Safety analysis

The safety analysis for the geological repository planned in Olkiluoto documents the scientific and technical understanding of the disposal system. This includes the safety barriers and safety functions that these are expected to provide, the results of a quantitative safety assessment, the process of analysing the ability of the repository system to maintain its safety functions and to meet the long-term safety requirements. Additionally, it provides a compilation of evidence and arguments that complement and support the reliability of the results of the quantitative analyses. [Posiva Oy, 2012]

2.1. Background of the research

The final disposal of nuclear fuel in Finland and Sweden is based on KBS-3V multiple barrier system which has been investigated extensively for its safety properties [Posiva Oy, 2012]. The quantitative safety assessment calculations extend to up to 10 000 years after the closure of the repository. In the long term, that is, after several thousands of years after the closure, the assessment is based on constraints on the release rates of the long-lived radionuclides of the nuclear fuel from the geosphere to the biosphere. In the very long term, after several hundred thousand years after the closure, no extensive quantitative safety assessment is required. Consequently, the judgement of safety is based on more qualitative considerations or complementary evaluations [Neall, F. et al., 2007].

The first barrier in KBS-3V system is the canister containing the nuclear fuel. The canister is made of iron inserts surrounded by copper overpack as a corrosion resistance and it is designed to last for as long as the nuclear fuel causes significant harm for the environment. A buffer consisted of swelling bentonite clay surrounds the canisters in the deposition tunnels preventing water intrusions to the copper canisters. The buffer also protects the canisters from comprising external stresses and limits the radionuclide releases in case of a leakage. The deposition tunnels are additionally to be backfilled, which again limits the radionuclide releases and contributes to the mechanical stability of the bedrock surrounding the repository system. Furthermore, the chemical composition of the nuclear fuel and its resistivity to dissolution provides an additional release barrier. Finally, the host rock provides isolation of the nuclear fuel from the surface environment

and the biosphere. A schematic diagram of the KBS-3V multiple barrier system is presented in Figure 2.1. [Posiva Oy, 2012]

The crystalline bedrock is the final barrier in the multiple barrier system and its retarding features have been investigated extensively in the Laboratory of Radiochemistry in the University of Helsinki. Three parameters that define the retention of radionuclides in the geosphere are diffusion coefficient, distribution coefficient and porosity. These parameters can be defined by experimental research and computer modelling and will be utilised in the safety calculations in the performance assessment of the final disposal of nuclear fuel. [Posiva Oy, 2012]

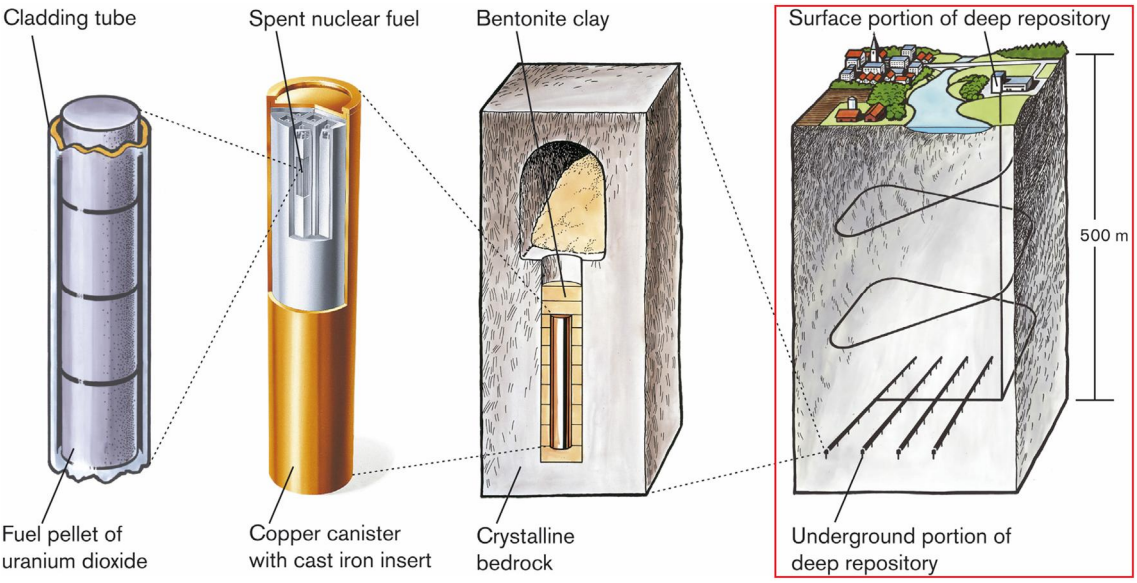

Fig 2.1. A schematic diagram of the multiple barrier system where the surrounding geosphere is the object of interest in this study. [Posiva Oy, 2012]

The safety calculations for the biosphere assessment include a screening process in which the radionuclides that could contribute to the total radiological impact are identified. The radionuclides that are considered as a potential radiological hazard are carried forward to detailed biosphere modelling taking into account the future landscape and ecosystem development over the next 10 000 years. This provides the framework for the modelling of radionuclide movements within the future surface environment and calculation of the radiation doses to, e.g. humans, plants and animals, inhabiting or utilising the various areas and resources that may be contaminated. [Posiva Oy, 2012]

2.2. Relevant nuclides in the final disposal of nuclear fuel

The radionuclides in the spent nuclear fuel to be deposited in the disposal system are located in the fuel, the fuel cladding, the matrix, the grain boundaries, cracks and gaps and in the materials of the assembly. The nuclides that are relevant for the long-term safety are the nuclides that might contribute to the overall doses to the biosphere in case of a leakage in the disposal system. The features that affect the relevancy of the radionuclides are, for example the chemistry, half-life and radiotoxicity [Posiva Oy, 2013; NEA, 2011]. The nuclides that are relevant for the long-term safety are presented in Table 2.1.

Table 2.1. The long-term safety relevant nuclides. [Posiva Oy, 2013]

Radionuclide	**Half-life [a]**
^{14}C	5700
^{36}Cl	3,01E+05
^{59}Ni	7,60E+04
^{79}Se	2,95E+05
^{90}Sr	28,9
^{91}Nb	680
^{92}Nb	3,47E+07
^{93m}Nb	16,12
^{94}Nb	2,03E+04
^{93}Mo	4000
^{99}Tc	2,11E+05
^{107}Pd	6,50E+06
^{108m}Ag	438
^{126}Sn	2,30E+05
^{129}I	1,57E+07
^{135}Cs	2,30E+06
^{226}Ra	1600
^{229}Th	7932
^{237}Np	2,14E+06
^{238}Pu	87,7
^{239}Pu	2,41E+04
^{240}Pu	6561
^{242}Pu	3,75E+05
^{241}Am	432,6
^{243}Am	7370
^{245}Cm	8423

Of the nuclides presented in Table 2.1., ^{14}C, ^{36}Cl and ^{129}I are placed in top priority class in the long-term safety according to the safety relevance in the biosphere. This is due to their non-sorbing nature which allows them to migrate relatively freely in the groundwater flow in case of a leakage in the repository [Posiva, 2009]. The migration behaviour of the top priority nuclides has been studied extensively in both laboratory and in-situ conditions [Tachi, Y et al., 2015; Soler, J.M. et al., 2015; Söderlund, M. et al., 2014]. High and medium priority nuclides, such as ^{135}Cs and ^{90}Sr, may have be of significant contribution to the dose in some calculation cases and their behaviour has also been under investigation [Muuri, E. et al., 2015; Kyllönen, J. et al., 2014; Wallace, S.H. et al., 2012]. In addition, it can be seen from Table 2.1. that ^{226}Ra is one of the long-term safety relevant nuclides due to its long half-life and high radiotoxicity. Although ^{226}Ra is placed in the low priority class, it has been stated that it can be of importance in the biosphere assessment [Posiva, 2009; Hedin, H. et al., 2013].

3. The chemistry and radiochemistry of the alkali earth metals

The group 2 or alkali earth metals are characterised with two electrons in their valence shell. Consequently, they form compounds in oxidation state +II and exist in aqueous solutions as M^{2+} ions. They are moderately electropositive and thus mostly form ionic compounds with the exception of beryllium that forms compounds with covalent bonds due to its small ion size [Lehto, J. and Hou, X., 2011]. The electropositivity and the ion size of alkali earth metals increases with atomic numbers. Alkali earth metals hydrolyse weakly although more readily than alkali metals. Furthermore, alkali earth metals do not readily form complexes with organic compounds because of the lack of vacancies in their electron shells to form coordination bonds with. [Greenwood, N.N. and Earnshaw, A., 1997]

Radium (Z=88) is an alkali earth metal with no stable isotopes. Its most important isotope is ^{226}Ra, which is originated from the decay chain of ^{238}U. ^{226}Ra decays by alpha decay to ^{222}Rn ($t_{1/2}$ = 1600 a) and gamma rays are also emitted in the process. However, the gamma radiation has so low an intensity (5.6 %) that the activity of ^{226}Ra cannot be determined utilising gamma spectrometry but alpha spectrometry must be utilised instead [Lehto, J.

and Hou, X., 2011]. The natural decay series in which ^{226}Ra appears, the uranium series, is presented in Figure 3.1.

In order to determine the alpha spectrum of ^{226}Ra it must be separated from its alpha emitting daughters with overlapping alpha peaks, e.g. ^{210}Po and the isotopes of uranium and thorium. The radiochemical separation of ^{226}Ra can be carried out using coprecipitation, ion exchange and solvent extraction methods [Lehto, J. and Hou, X., 2011]. Because radium has no stable isotopes and no suitable radioactive tracer, stable barium is used as a carrier and stable barium or gamma emitting ^{133}Ba as a yield determinant [Juntunen, P. et al., 2001]. Radium does not form anionic complexes in nitric or hydrochloric acid and cannot be removed with anion exchange. However, anion exchange can be utilised in removing interfering nuclides, such as ^{210}Po or ^{238}U. In addition, radium does not readily form organic complexes and cannot be removed with solvent extraction but, again, interfering nuclides can be separated utilising the technique. Moreover, Ra^{2+} ions bind to cation exchangers which can be utilised in the separation of radium.

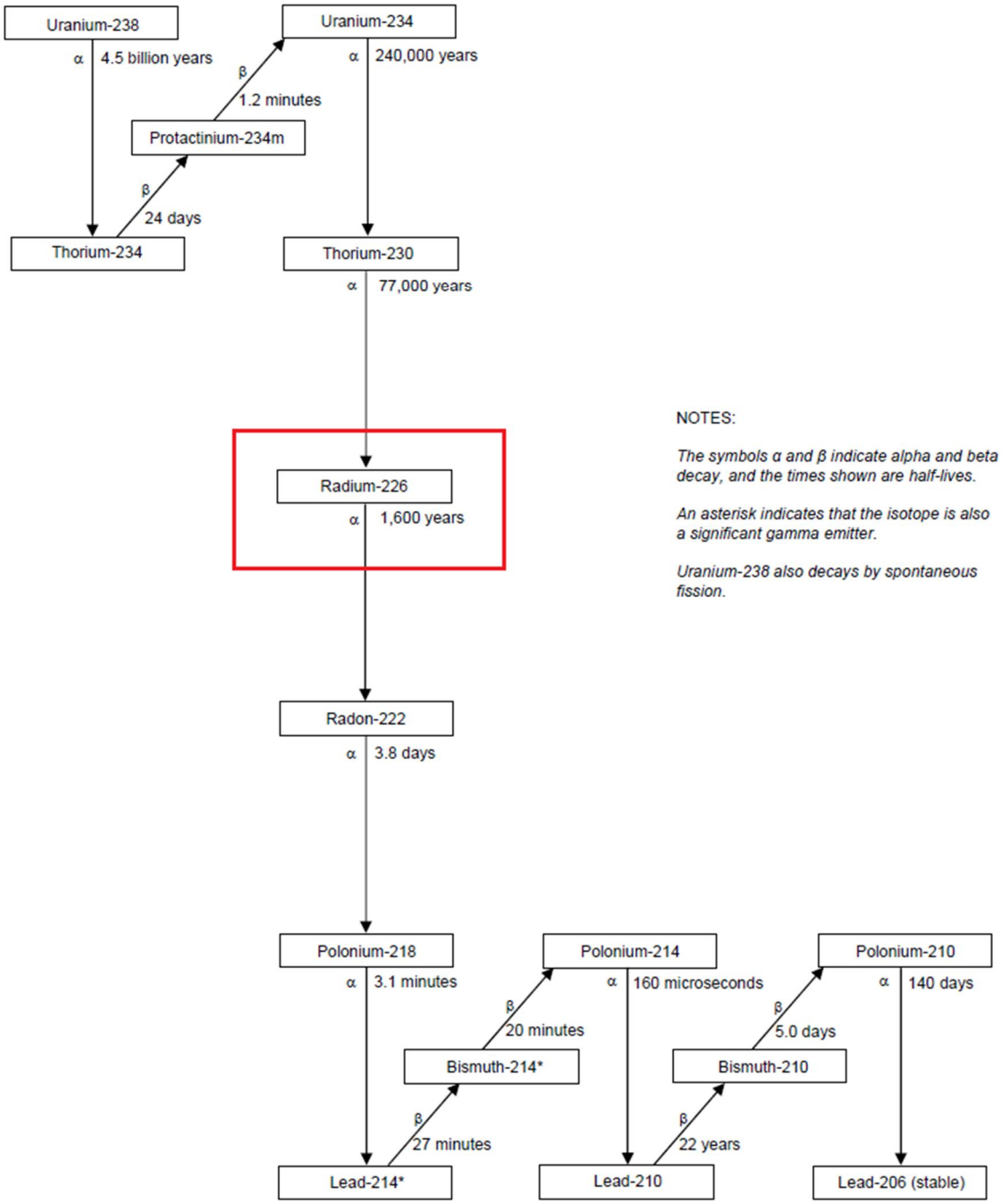

Fig 3.1. The uranium series where ^{226}Ra is indicated. [Peterson, J. et al., 2007]

Barium (Z=56) is also an alkali earth metal. Radioactive isotope ^{140}Ba ($t_{1/2}$=12.8 d) with a high fission yield (6.21 %) [Celebi, O. et al., 2009] is present in nuclear fuel and is a serious contaminant although it is only significant in the first months after the nuclear fuel has been taken out of the reactor and will thus not end up into the repository [Shahwan, T. and Erten, H.N., 2004]. In addition, barium has been widely used as an

analogue for radium because of its chemical similarity. Whereas the separation of ^{226}Ra is time-consuming and laborious, no radiochemical separation is needed for the gamma emitting ^{133}Ba [Celebi, O. et al., 2009]. The radiochemical characteristics of the most important nuclides of barium and radium are shown in Table 3.1.

Table 3.1. Important radionuclides of barium and radium. [Lehto, J. and Hou, X., 2011]

Nuclide	Half-life	Decay mode	Gamma emission	Source or use
^{133}Ba	10.7 a	EC	yes	tracer, activation product
^{140}Ba	13 d	β^-	yes	fission product
^{226}Ra	1600 a	α	yes	natural nuclide
^{228}Ra	5.8 a	β^-	no	natural nuclide

Additionally, the ionic radii of Ba^{2+} and Ra^{2+} are similar to each other. Furthermore, the ionic radii are similar to many abundant ions in common minerals, for example Ca^{2+} and K^+. This allows the ion exchange process to occur between ions with similar ionic radii and charge. Ion exchange is a highly important factor in retaining radionuclides in the geosphere [Molinero, J. and Samper, J., 2006]. The ionic radii of Ba^{2+}, Ra^{2+} and common cations in minerals are presented in Table 3.2.

Table 3.2. The ionic radii of Na^+, Mg^{2+}, K^+, Ca^{2+}, Ba^{2+} and Ra^{2+}. [Shannon, R.D., 1976]

	Na^+	Mg^{2+}	K^+	Ca^{2+}	Ba^{2+}	Ra^{2+}
Atomic number	11	12	19	20	56	88
Ionic radium (6 coord) [pm]	102	72	138	100	135	148

4. The geology and mineralogy of the Grimsel and Olkiluoto site

4.1. Grimsel site

The Grimsel test site is located at an altitude of 1,730 m in the granitic rock of the Aare Massif in central Switzerland [Tachi, Y. et al., 2015]. The Aare Massif is consisted of a metasedimentary envelope that was intruded by Hercynian granitoids (320-280 Ma). In addition, all the rocks in the area have been affected by Alpine greenschist metamorphism and deformation (25 Ma) and the post-metamorphic regional uplift that is still ongoing, currently 1-2 mm/a [Möri, A. et al., 2003]. The bedrock in the Grimsel test site area is composed of granodiorite [Hoehn et. al, 1998] and Aare granite [Hu, Q. and Möri, A.,

2008]. The mineralogical composition of granodiorite is presented in Table 4.1. Grimsel granodiorite is homogeneous, medium grained and slightly preferentially-oriented (foliation). In addition, it contains brittle structural features of cataclastic fault breccias and discrete faults [Möri, A. et al., 2003] The main minerals of granodiorite are quartz (30-40 %), plagioclase (30-40 %), potassium feldspar (10-20 %) and biotite (5-10 %) and their crystallographic structures from SHAPE software are shown in Figure 4.1. Other minerals, which do not exceed 5 % in volume, are green amphibole (hornblende), muscovite, epidote, titanite and opaque minerals which are most probably iron sulphides like pyrite [Jokelainen et. al, 2013]. The main minerals of granodiorite were chosen for the batch sorption experiments.

Table 4.1. The mineralogical composition of two granodiorite samples from the Grimsel study site. Volume-% is calculated by point counting method, 500 points/ thin section [Jokelainen et. al, 2013].

Mineral	**Sample 1 B Vol. %**	**Sample 2 B Vol. %**
Plagioclase	39.0	34.0
Quartz	28.4	37.2
Potassium feldspar	21.6	12.8
Biotite	5.0	7.8
Muscovite		
Sericite	2.6	1.6
Epidote	1.2	1.0
Amphibole	1.8	4.6
Chlorite	0.2	0.4
Carbonate		
Titanite	+	0.6
Apatite		
Opaque minerals	0.2	+

+ optically observed

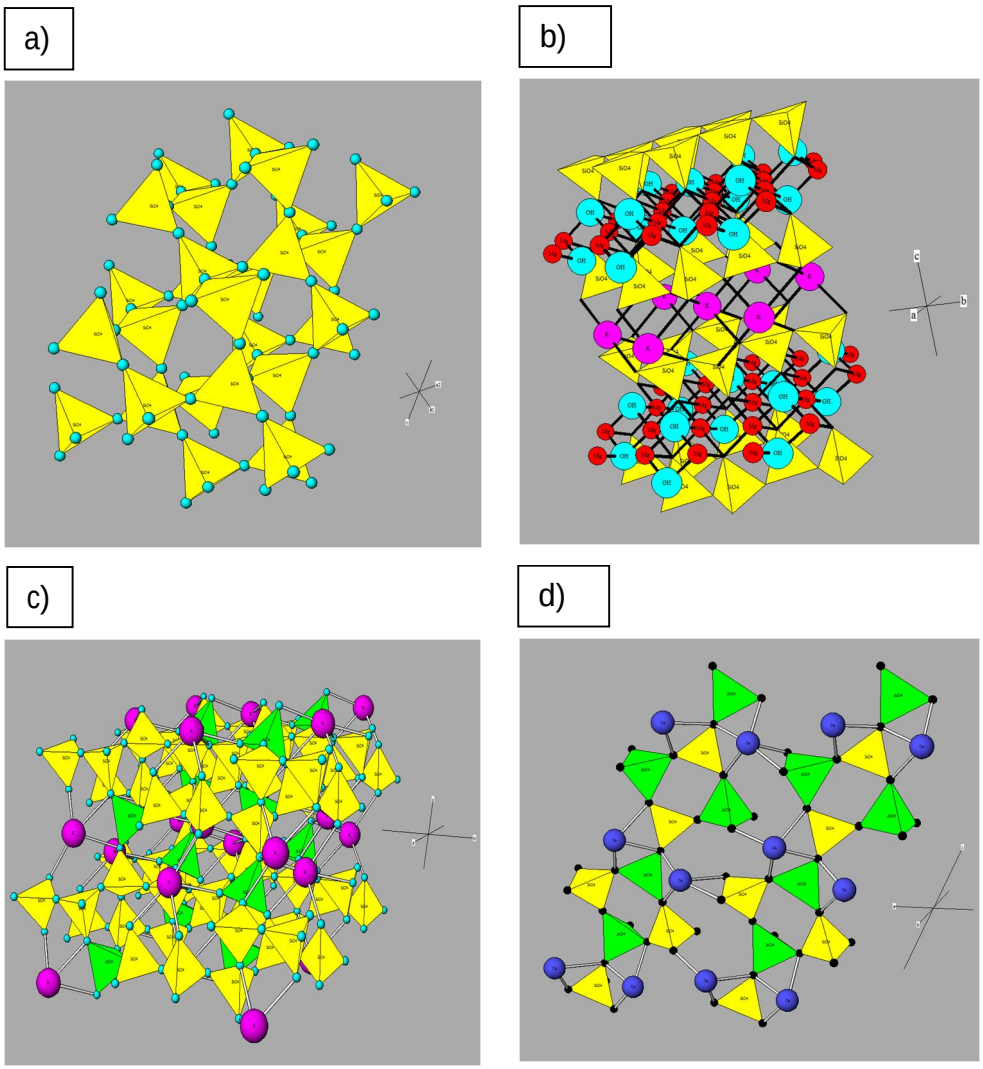

Fig 4.1. The crystallographic structures of **a)** quartz, **b)** biotite, **c)** potassium feldspar and **d)** plagioclase from SHAPE software.

The chemical formula of quartz is SiO_2, whereas the chemical composition of biotite varies significantly in different conditions and its approximate chemical formula is $K(Mg,Fe)_3(AlSi_3O_{10})(F,OH)_2$. The chemical formula of potassium feldspar is $KAlSi_3O_8$ and that of plagioclase is $CaAl_2Si_2O_8$ (anorthite) or $NaAlSi_3O_8$ (albite) [Klein, C. and Dutrow, B., 2007]. The main cations in the structure of biotite are thus potassium and magnesium, whereas in potassium feldspar they are potassium and in plagioclase calcium (anorthite) and sodium (albite). Furthermore, quartz is only consisted of silicon and oxygen. The ionic radii of Ca^{2+}, Ba^{2+} and Ra^{2+} are relatively similar (Table 3.2.) and they

can thus be exchanged by each other in the exchange sites of the minerals, which are usually located in the edges or interlayers of the crystal surfaces.

4.2. Olkiluoto site

The Olkiluoto site is an island located on the coast of south-western Finland and the repository system is built in the depth of 400 m below the surface. The site is situated in the part of the Fennoscandian shield where the postglacial land uplift is moderate, about 6 mm per year. The latest glaciation in southern Finland lasted over 50 000 years and the ice sheet retreated from the Olkiluoto site about 10 000 years ago leaving the area sub aquatic. [Pitkänen, P. et al., 1996]

The bedrock in the area is of Archaean, good quality crystalline but heterogeneous rock. The degree of heterogeneity and foliation change rapidly in the bedrock in Olkiluoto area. The main rock type in the depth of the deposition facility is veined gneiss (43 %) with shorter sections of pegmatite (20 %). Veined gneiss shows a high level of deformation with powerful foliation whereas pegmatite can be found as coarse-grained irregular masses. The main minerals of veined gneiss are quartz, plagioclase, biotite and potassium feldspar whereas the main minerals of pegmatite are quartz, plagioclase and potassium feldspar. The average mineral compositions of veined gneiss and pegmatite are presented in Table 4.2. [Posiva Oy, 2009; Kärki, A. and Paulamäki, S., 2006]

Table 4.2. The average mineral compositions of veined gneiss and pegmatite and their standard deviations. [Kärki, A. and Paulamäki, S., 2006]

Mineral	**Veined gneiss**		**Pegmatite**	
	AVG	STD	AVG	STD
Quartz	20.8	12.7	35.2	14.3
Plagioclase	22.6	16.6	16.7	8.5
Potassium feldspar	6.9	8.4	32.8	17.6
Biotite	20.2	14.3	0.9	1.7
Muscovite	3.9	5.4	2.5	2.8
Hornblende	4.1	9.9	0.0	0.0
Pyroxene	0.1	0.1	0.0	0.0
Chlorite	3.7	8.3	0.7	0.9
Cordierite	0.2	0.3	0.1	0.4
Pinite	5.5	9.9	0.4	1.7
Garnet	0.1	0.1	0.4	1.0
Sillimanite	0.1	0.1	0.4	1.3
Epidote	0.1	0.1	0.0	0.2
Sphene	0.2	0.4	0.0	0.0
Apatite	2.1	3.2	0.0	0.1
Saussurite	2.3	2.8	7.5	5.9
Sericite	2.0	4.7	1.2	2.9
Opaques	0.9	1.3	0.4	0.5

5. The retention of radionuclides in crystalline rock

If a leakage should occur in the canisters of the repository, radionuclides would be transported by the flowing groundwater in the fractures of the rock, which are macroscopic openings caused by stress. However, a significant retention of radionuclides from the flow in the bedrock will occur if the nuclides are able to diffuse into the pore space of the rock matrix and the microscopic fissures of the rock. In such a situation diffusion acts as a retarding mechanism which can remove some of the nuclides from the flowing groundwater into the micropores of the rock matrix and fissures of the host rock. Additionally, nuclides that are sorbed on the fracture surfaces and their altered minerals can be sorbed also on the pore surfaces of the host rock in addition to the fissure surfaces increasing the retention. Thus, the main processes of radionuclide retention from flow are diffusion and sorption. [Skagius, K. and Neretnieks, I., 1988]

5.1. Flow

Groundwater in the soil and in the bedrock is formed as a consequence of infiltration of precipitation into the soil and, finally, the bedrock. In case of a leakage in the repository system the radionuclides would migrate with the groundwater flow path and in fractured rocks flow takes place in channels within the fractures [Moreno, L. et al., 2006; Smith, P.A. et al., 2001]. The nuclides may become sorbed on the mineral surfaces along the flow which retards the transport of the nuclides in comparison with the flow velocity of the groundwater. In a slow flow rate the residence time is longer and there is more time for the nuclides and mineral surfaces to react and the retardation of radionuclides is thus more preferential. [Appelo, C.A.J. and Postma, D., 2005]

The hydraulically conductive network in the bedrock is formed from the geological environment of hard fractured rocks together with the more intensively fractured zones. All fractures do not, however, conduct water and according to several studies performed in hard rock environments of the bedrock the majority of fractures may not be hydraulically active. However, it is quite certain that all fractures are water saturated. Consequently, to understand the groundwater flow certain parameters must be well characterised from the geological environment. In-situ information on the fracture properties can be gathered with hydraulic experiments and regarding the flow, as well as transport, transmissive properties of fractures need to be characterised. [Öhberg, A. and Rouhiainen, P., 2000]

The flow concentrates dynamically to a high degree on some limited areas although the fracture plane itself may be hydraulically well connected over large areas. As a consequence, in a major part of the fracture, water moves very slowly or, in fact, not at all. In crystalline rock the fracture network and its hydraulic properties control the flow on a larger scale and this, in turn, depends on the structural and mineralogical properties of the individual fractures in the host rock. To predict the flow in a fracture, the knowledge of the fluid property, the boundary conditions, and the fracture void geometry is required. Consequently, 3D distributions of minerals and porosities of the rocks in Grimsel and Olkiluoto have been analysed using conventional petrography methods, electron microscopy, ^{14}C-PMMA porosity analysis and X-ray tomography. [Öhberg, A. and Rouhiainen, P., 2000; Kuva, J. et. al., 2012]

5.2. Diffusion

In general, transport by advection dominates in zones of high hydraulic conductivity, such as fractures in the rock matrix. However, in materials of very low conductivity diffusion is the dominant transport process. Thus, for predicting the transport of nuclides from the nuclear fuel in case of a leakage, a detailed understanding of diffusion processes in natural geological materials is essential [Boving, T. and Grathwohl, T., 2001].

Molecular diffusion is a process in which a concentration difference between two points in a stagnant solution will be evened by the random Brownian movement of molecules in time [Appelo, C.A.J., Postam, D., 2005]. As a consequence, the medium in which the diffusion occurs does not move but only the materials distributed unevenly in the medium due to the gradient of the concentration [Stegena, L., 1983] Diffusion is generally described by Fick's laws and the first Fick's law relates the flux of a chemical to the concentration gradient:

$$F = -D_{eff}\frac{\partial c}{\partial x} \qquad 5.1.$$

where F is the flux (mol/s/m^2), De_{ff} is the effective diffusion coefficient (m^2/s), and c is the concentration (mol/m^3). [Cussler, E.L., 2009]

In this work the diffusion is studied in the pore space of porous media, rock. Effective diffusion coefficient takes into account also the porosity of the rock and it can be defined as:

$$D_{eff} = \frac{D_{aq}\varepsilon_{eff}\delta}{\tau_f} \qquad 5.2.$$

where D_{aq} is the aqueous diffusion coefficient in pure water, ε_{eff} is the effective porosity of the rock and τ_{f} is the tortuosity factor of the rock. The effective porosity accounts for the reduced cross-sectional area available for diffusion in the pore space and the tortuosity factor is a geometric parameter and accounts for the pore space geometry [Boving, T. and Grathwohl, T., 2001].

Thus, the Fick's first law predicts how much of the flux can be expected. Fick's second law, on the other hand, is more specified and it predicts the rate at which the concentration is changing in the system. Fick's second law can be presented as:

$$\varepsilon \frac{\partial c}{\partial t} = D_{eff} \frac{\partial^2 c}{\partial x^2} - \rho \frac{\partial q}{\partial t} \quad 5.3.$$

where ρ is the bulk density of the porous medium and q is the sorbed concentration in the porous medium. The term $\partial q / \partial t$, on the other hand, represents a sink term due to the sorption of the solute [Boving, T. and Grathwohl, T., 2001].

If the relationship between the sorbed concentration (q) and the concentration of the solute in solution (C) is linear and the local equilibrium assumption, where reversible sorption reactions are assumed to be in local chemical equilibrium is valid, then the distribution coefficient ($K_d=q/C$) may be used to express the Fick's second law as:

$$\frac{\partial c}{\partial t} = \frac{D_{eff}}{\varepsilon + K_d \rho} \frac{\partial^2 c}{\partial x^2} \quad 5.4.$$

where ε is the porosity of the rock. The term ($\varepsilon+K_d\rho$) in the equation is known as rock capacity factor α. Furthermore, the term ρK_d equals zero if no sorption or retardation occurs and the rock capacity factor α is then, consequently, equal to the total porosity [Boving, T. and Grathwohl, T., 2001]. The ratio D_{eff} / α can be denoted as the apparent diffusion coefficient (D_{app}):

$$D_{app} = \frac{D_{eff}}{\alpha} = \frac{D_{aq} \varepsilon_{eff}}{(\varepsilon + K_d \rho) \tau_f} \quad 5.5.$$

When the apparent diffusion coefficient is defined as the effective diffusion coefficient divided by the rock capacity factor, it takes into account both the matrix porosity and the different chemical sorption behaviour of different radionuclides.

5.3. Sorption

Sorption is either a chemical or a physical process in which a solute is transferred from the solution to the solid phase. As a broad definition, sorption includes absorption, adsorption and coprecipitation. However, coprecipitation will not be covered in the following section. In the case of trace elements in groundwater, the dominant process is adsorption. In batch sorption experiments sorption can be described with the distribution coefficient:

$$K_d = \frac{C_m}{C_s} \quad 5.6.$$

where C_m is the concentration in mineral and C_s is the concentration in solution. The distribution coefficient is strongly dependent on the chemistry of the groundwater and the nature of the sorbing ion and must thus be determined separately for different ions. Mineral surfaces are commonly described as generic hydroxylated surface groups, S-OH with amphoteric character due to which they can act as both acids and bases depending on the pH of the solution [O'Day, P., 1999]. At low pH the surface protonates as $S\text{-}OH_2^+$ and the surface is positive, whereas at high pH the surface dissociates as $S\text{-}O^-$ and the surface is negative. Thus, at low pH the sorption of anions is preferred and at high pH the sorption of cations is preferred. As a result, hydration and complexation affect the sorption behaviour of an ion dramatically.

Adsorption is a process in which a solute is retained on the surface of a solid phase. It can take place chemically through covalent bonding which is also called chemisorption. Additionally, adsorption can occur physically through electrostatic interactions (dipole-dipole, ion-dipole, van der Waals forces) which is called physisorption. In chemical adsorption inner sphere complexation occurs where the metal ion loses parts of its hydration shell and a chemical bond is formed between the sorbing ion and the mineral surface [Cole, D.R., 1983; Stumm, W., 1992]. In physical adsorption an outer sphere complex is formed where the hydration sphere of the sorbing ion is retained in the attachment on the mineral surface [Stumm, W., 1992]. Adsorption can also be further divided to ion exchange and surface complexation.

Ion exchange involves the replacement of one ion bound electrostatically at a surface of a solid structure with another one of the same sign. Ion exchange is, thus, a sorption process in which outer sphere complexes are formed [Fernandes, M.M. and Baeyens, B., 2012]. The ion exchange processes can be described as binary ion exchange reactions according to the Gaines-Thomas convention [Appelo and Postma, 2005]. In this approach the cation exchange reaction is written with the cation exchange sites (X^-) as:

$$2Na - X + Ba^{2+} \leftrightarrow Ba - X_2 + 2Na^+ \qquad 5.7.$$

The distribution of species and the selectivity coefficient can thus be represented as:

$$^{Ba}_{Na}K_c = \frac{[Ba-X_2][Na^+]}{[Na-X][Ba^{2+}]^{0.5}} = \frac{\beta_{Ba}^{0.5}[Na^+]}{\beta_{Na}[Ba^{2+}]^{0.5}} \qquad 5.8.$$

where X^- is the cation exchange site and β is the equivalent fraction of the exchangeable ions as a fraction of the total. In the reaction, Ba^{2+} is taken up by the exchanger as the two Na^+ ions are released. The K_c value represents the selectivity of a particular ion exchange process and a higher K_c value suggests a higher affinity or selectivity for the exchanging cation and thus higher sorption. A schematic picture for ion exchange process is presented in Figure 5.1.

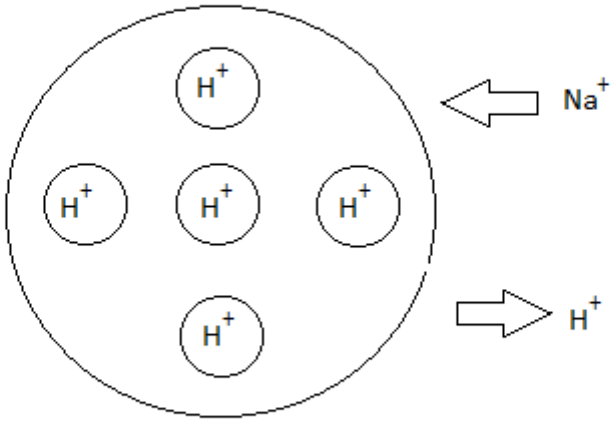

Fig 5.1. A schematic picture for ion exchange process.

Generally in sediments and soils, the selectivity of ions follows the lyotropic series, that is, cations with the same charge are more strongly attached when their hydration number decreases. Thus, when the hydration shell of water molecules around the ion is smaller the sorption is more vigorous and more selective. A similar behaviour can also be seen for synthetic, strongly acidic ion exchange resins. This, on the other hand, suggests that the majority of the cation exchangers in the environment can act similarly as strongly acidic cation exchangers. [Appelo and Postma, 2005]

The composition of a cation exchanger in the bedrock will be in equilibrium with the resident groundwater under steady-state conditions. However, when the composition of the water changes abruptly as a result of, for example, a leakage in the final disposal facility, the cation exchanger readjusts its composition to the new groundwater

composition. The exchanger thus acts as a temporary buffer which may retard the nuclides from leakage in the repository. [Appelo and Postma, 2005]

In surface complexation an ion is attached on the surface of a mineral with an inner sphere or an outer sphere complex. Inner sphere complexation takes place as ions with high affinity for the surface lose a part of their hydration shell and form a chemical bond between the sorbing ion and the surface hydroxyl group. As a result, the sorbing ion replaces a reactive surface hydroxyl from the surface hydroxyl group [Nagata, T., and Fukushi, K., 2010]. Outer sphere complexes contain at least one water molecule between the adsorbing ion and the surface hydroxyl group and the attachment is dominated by dipole-dipole or ion-dipole interactions. A schematic picture of surface complexation is presented in Figure 5.2.

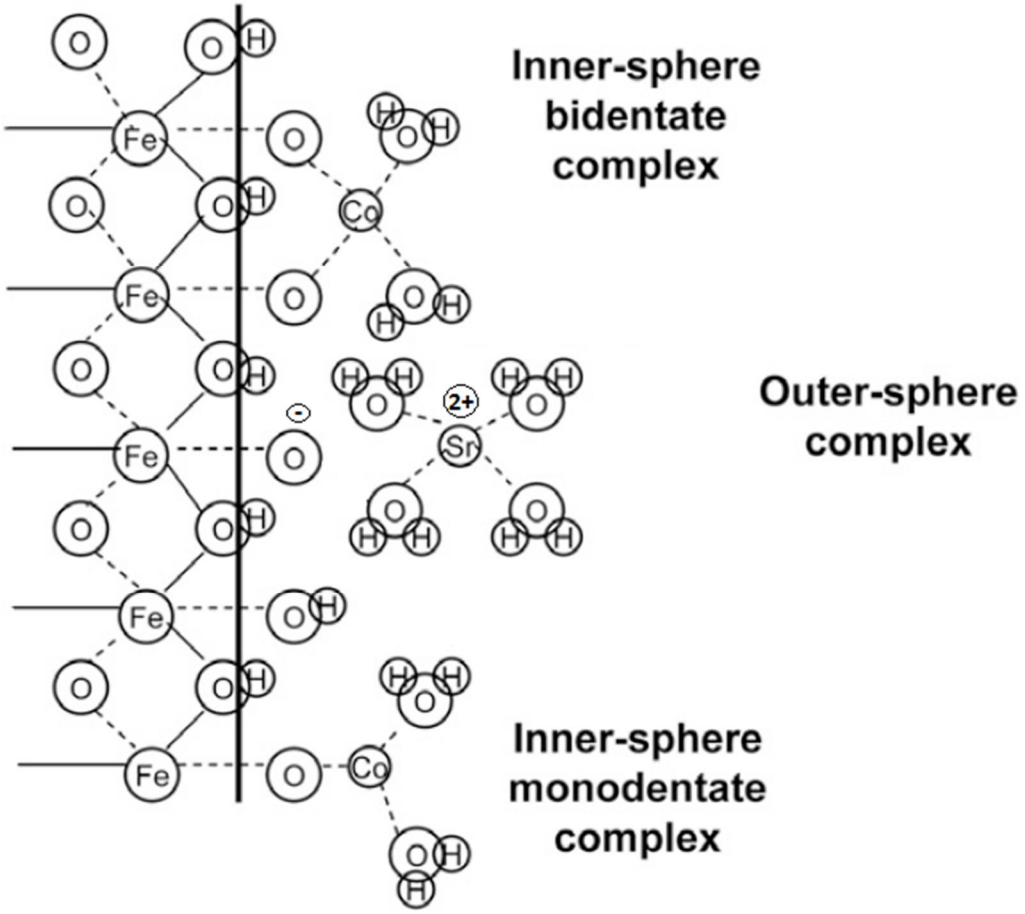

Fig 5.2. A schematic picture of surface complexation. [Goldberg, S. et al., 2007]

For example, it has been studied that as a large ion (see Table 3.2.) Ba^{2+} sorbs on the surface of ferrihydroxide minerals as tetradentate complexes likely by outer sphere mechanism by surface reactions [Sajih, M. et al., 2014]:

$4 \equiv SOH + Ba^{2+} \rightarrow [(\equiv SOH)_3(\equiv SO)Ba]^+ + H^+$

$4 \equiv SOH + Ba^{2+} + 2H^+ \rightarrow [(\equiv SOH_2)_2(\equiv SOH)_2Ba]^{4+}$

where ≡SOH denotes surface hydroxyl. The surface complexation of barium has been discovered to be fully reversible [Sajih, M. et al., 2014].

The sorption of barium has been discovered to occur both via ion exchange and surface complexation [Sugiyama, S. et al., 2000; Sajih, M. et al., 2014]. However, it has been discovered that ion exchange is the dominant sorption process for barium and surface complexation can be ignored in the model because of its low significance.

6. Modelling

6.1. Sorption

6.1.1. Adsorption isotherms

Sorption is frequently described by isotherms showing the relationship between the concentration of adsorbate and the total concentration adsorbed at a constant temperature. Isotherms do not take kinetic aspects into account but they rather describe equilibria. The simplest isotherm is Langmuir isotherm assuming that the adsorption sites, S, on the surface of a solid become occupied by the adsorbate, A, from the solution. It is based on the assumptions that the adsorption is in equilibrium up to the formation of a monolayer coverage and all surface sites have equal activity [Stumm, W. and Morgan, J.J., 1996] The Langmuir equation can be derived for a surface adsorption reaction:

$$S + A \leftrightarrow SA \qquad 6.1.$$

where the law of mass action derives:

$$\frac{d[SA]}{dt} = k_1[SA] - k_{-1}[SA] = 0 \text{ at equilibrium} \qquad 6.2.$$

where k_1 is the forward rate constant and k_{-1} is the backward rate constant. The equilibrium constant K_{ads} can be concluded as:

$$K_{ads} = \frac{[SA]}{[S][A]} = \frac{k_1}{k_{-1}} = e^{-\frac{\Delta G^{\circ}_{ads}}{RT}} \qquad 6.3.$$

From mass balance principles, the maximum concentration of surface sites (Γ_{max}) is [Stewart, B.A., 1999]:

$$\Gamma_{max} = \Gamma_0 + \Gamma_A \quad 6.4.$$

where $\Gamma_A=[SA]$ and $\Gamma_0=[S]$. By combining equations 6.3. and 6.4., Langmuir equation can be presented as a function of the total number of sorption sites (Γ_{max}):

$$\Gamma_A = \frac{\Gamma_{max}K[A]}{1+K[A]} \quad 6.5.$$

where K is the equilibrium constant.

As the Langmuir isotherm assumes that the sorption sites are fully saturated after a monolayer coverage, no further sorption can occur even though the concentration of adsorbate would increase. Freundlich isotherm is another adsorption isotherm that can also take into account the sorption with unlimited sorption sites [Sheha, R.R. and Metwally, E., 2007]. The Freundlich equation is presented, respectively, as:

$$\Gamma = m[A]^n \quad 6.6.$$

where Γ is the quantity of the sorbate associated with the sorbent, $[A]$ is the total concentration of the sorbate in solution, m is the Freundlich constant and n is the measure of nonlinearity involved. The Freundlich equilibrium constant, K_{ads}, can be presented as:

$$K_{ads} = \frac{[SA]}{[A]^{\frac{1}{n}}} \quad 6.7.$$

The adsorption isotherms are commonly used in describing the equilibrium nature of adsorption processes in heterogeneous systems. These equations, however, have serious limitations in their usage and cannot be used in, for example, broad concentration ranges [Sheha, R.R. and Metwally, E., 2007]. Consequently, more discrete computational models have been developed to describe the processes in greater detail.

6.1.1. Ion exchange modelling

PHREEQC [Parkhurst and Appelo, 1999] is a geochemical modelling code that can simulate a variety of geochemical processes including water and mineral equilibriums, ion exchangers, surface complexes, etc. Ion exchange can be modelled with the PHREEQC software using the Gaines-Thomas convention presented in equation 5.8. However, PHREEQC handles the exchange reactions by splitting them into two half reactions. In addition, the selectivity coefficients for different ion exchange reactions can be derived from the equilibrium constants of the half reactions. For example, we can rewrite the example given in equation 5.7.

$$2Na - X \; + \; Ba^{2+} \leftrightarrow \; Ba - X_{\,2} \; + \; 2Na^{+} \qquad 6.8.$$

When the selectivity coefficient $K_{Na/Ba}$ is 0.35 [Appelo, C.A.J., Postma, D., 2005], the log $K_{Ba/Na}$ value equals log K = log (1 / $K^2_{Na/Ba}$) = log (1 / 0.35^2) = 0.91. One of the half reactions needs to be defined as the point of reference:

$$Na^{+} + X^{-} \leftrightarrow Na - X; \qquad \log K = 0.0 \qquad 6.9.$$

By adding the reaction 6.9. twice to the reaction 6.8., we obtain:

$$Ba^{2+} + 2X^{-} \leftrightarrow Ba - X_2; \quad \log K = 0.91 \qquad 6.10.$$

which is the equation used in the PHREEQC database to describe the ion exchange of the Ba^{2+} cation. The log K values are provided as coefficients rather than constants since the values depend on the composition of the exchanger present in the bedrock, which is not constant. The selectivity coefficients of the exchange reactions are thus usually given as a range that represent different conditions. [Appelo, C.A.J., Postma, D., 2005]

In PHREEQC, there are different keywords, under which investigated geochemical reactions can be defined. For example, in the database of the PHREEQC software, the exchanger *X* is specified under the keyword EXCHANGE_MASTER_SPECIES and the exchange half-reactions are given under the keyword EXCHANGE_SPECIES. The same activity coefficient is used in the software for the exchangeable species as for the aqueous species due to experimental observations of Na^+/Ca^{2+} exchange in saline soils [Appelo, C.A.J., Postma, D., 2005]. This can lead to the overestimation of monovalent ion exchange compared to divalent ion exchange, which can be avoided by calculating the exchanger composition in contact with the investigated groundwater.

In addition, the keyword EXCHANGE is used to define the amount and assemblage of the ion exchanger in the investigated conditions. The initial composition of the exchange assemblage can be defined by explicitly listing the composition of each exchange component or through parameter optimisation. Additionally, the initial composition of the exchanger can be defined by implicitly specifying that the exchanger is in equilibrium with the investigated solution with a fixed composition. The stoichiometry of the exchanger and the exchange sites is also defined under the keyword EXCHANGE. [Appelo, C.A.J., Postma, D., 2005; Parkhurst, D.L. and Appelo, C.A.J., 1999]

It has been studied extensively, that a three site model [Bradbury, M.H. and Baeyens, B., 2000] can be employed to the sorption studied of caesium on biotite and biotite rich rocks [Kyllönen, J. et al., 2014; Muuri, E. et al., 2015]. In the model, there are assumed to be three different sorption sites, each of which having different capacities and affinities. The three sorption sites are generally divided into high and low affinity sites, where the high affinity sites are, furthermore, divided in two to give a frayed edge site (FES) and Type II sorption site. The low affinity sites are referred to as planar sites. [Bradbury, M.H. and Baeyens, B., 2000]. Additionally, the three site model has also been applied to the sorption behaviour investigation of alkali earth metals [Ferrell, R.E. et al., 2002; Tertre, E. et al., 2009].

The FES are commonly defined to be as a partially expanded wedge zone at the edge of the interlayer of the sheet structure having a basal spacing of 10-14 Å [Fuller, A.J. et al., 2014]. They are formed when the mica minerals undergo weathering expanding the edge inwards. It has been discovered that the FES are selective for weakly hydrating ions and their existence has been verified by X-ray microprobe methods [McKinley, J.P. et al., 2004]. It has been discovered that the proportion of the FES of the total ion exchange capacity vary between 0.02 % and 0.5 % [Kyllönen, J. et al., 2014].

The Planar sites are located on the basal plane of the mineral structure making up for the majority of the total ion exchange capacity and they are much less selective than the FES. However, the physical background of the Type II sites is still unclear. It has been discovered that the use of Type II sites in the modelling improves the fit with the experimental data but their contribution to the total ion exchange capacity has varied from 0.26 % to 28 % [Kyllönen, J. et al., 2014]. It has been generally considered that the Type II sites are located further out in the wedge where the interlayer is fractionally expanded [Bradbury, M.H. and Baeyens, B., 2000; Fuller, A.J. et al., 2014].

6.1.2. Surface complexation modelling

Surface complexation has been commonly described by two types of models: the two layer model and the triple layer model. In the two layer model the diffuse double layer is defined to start immediately at the charged surface and thus the surface potential is directly connected to the surface charge via the capacitance. The capacitance can be defined by the user in constant capacitance model and by the ionic strength in the double layer model via the Gouy-Chapman relation:

$$\sigma_{DL} = 0.1174\sqrt{I} \cdot \sinh\left(\frac{F\psi_0}{2RT}\right) \qquad 6.11.$$

where σ_{DL} is the charge of the double layer, I is the ionic strength, F is Faraday's constant, R is the gas constant, T is temperature and ψ_0 is the potential. The two layer model is the simplest of the surface complexation models. [Appelo, C.A.J., Postma, D., 2005]

In the three layer model three different layers with different capacitances are assumed. One compact layer starting at the surface is called Stern layer, another layer is starting at a closest approach distance and the last layer is more corresponding with the diffuse double layer. Three capacitances must be defined in the model for the three corresponding layers but commonly only the one for the Stern layer is adjusted as the capacitances for the other layers are assumed constant. [Appelo, C.A.J., Postma, D., 2005; Hayes, K.F. et al., 1991]

In both models the composition of the diffuse double layer is completely ignored and they only consider the complexed ions and not the electrical work regarding the surface complexation. However, most chemical observations can be described well with both models. The triple layer model has more options to account for the details in the surface complexation processes but it is much more complex and is thus rarely used. The two layer model offers an adequate estimation for most of the experimental studies. The double layer model is included in the PHREEQC software [Appelo, C.A.J., Postma, D., 2005]. The surface complexation model can be employed in the investigation of the sorption properties of barium in, for example, soils [Catalette, H. et al., 1998].

6.2. Diffusion

6.2.1. PHREEQC

PHREEQC software includes capabilities to simulate dispersion or diffusion in one-dimensional transport calculations with or without advective transport. The 1D transport model can be constructed under the TRANSPORT keyword and it can be coupled with the ion exchange model to take the retention of radionuclides into account in the transport model. The molecular diffusion model under the TRANSPORT keyword is described by the advection-reaction-dispersion (ARD) equation
[Parkhurst, D.L. and Appelo, C.A.J., 1999; Appelo, C.A.J., Postma, D., 2005]:

$$\left(\frac{\partial c}{\partial t}\right)_x = -v\left(\frac{\partial c}{\partial x}\right)_t - \left(\frac{\partial q}{\partial t}\right)_x + D_L\left(\frac{\partial^2 c}{\partial x^2}\right)_t \qquad 6.12.$$

where c is solution concentration, q is the solid concentration, D_L is the dispersion coefficient and v is the velocity of a given concentration.

The flow line in the transport model is discretised in a number of cells with a given length. A specified number of shifts move the cell contents to the higher numbered cells so that the investigated groundwater will migrate for the length of all the defined cells. In addition to the cell length and their quantities also diffusion coefficient, time step and dispersivity must be defined [Parkhurst, D.L. and Appelo, C.A.J., 1999]. The transport model in PHREEQC can be employed to study the penetration depth of diffusion [Ferrell, R.E. et al., 2002].

6.2.2. Comsol

COMSOL Multiphysics is a software platform for modeling and simulating physics-based problems and it is based on advanced numerical methods. Coupled or multiphysics problems, including matrix diffusion, can be modelled using the software. [Comsol, 2012]

Transport of diluted species through porous media is usually treated using simplified homogeneous models with effective transport properties. This is a necessity for modelling transport in microfractures of the bedrock would be too demanding to compute. The transport of diluted species interface under the chemical species transport branch in the

software provides a predefined modelling environment convenient for studying the evolution of chemical species transported by diffusion. In the interface, all solutes are presumed to be diluted and the model can be constructed in 1D, 2D or 3D. [Comsol, 2012]

When the transport mechanism of the solute is assigned to be diffusion only the mass balance equation assumed in the interface becomes:

$$\frac{\partial c}{\partial t} = \nabla \cdot (D \nabla c) + R \qquad 6.13.$$

where c is the concentration of the species, D denotes the diffusion coefficient and R is a reaction rate expression for the species. In the transport of diluted species interface, Fick's laws describe the diffusive transport in the flux vector which is adequate when the diffusing species is dilute with respect to a solvent, that is, when the transported species have concentrations at least an order of magnitude less than the solvent. [Comsol, 2012]

6.2.3. Time-domain-diffusion modelling

Time-domain-diffusion (TDD) is a modelling method that takes into account the 3D heterogeneity of the rock matrix. The TDD method calculates the diffusion time between the centres of two adjacent voxels in one step. In the method a particle is forced to jump at each simulation step to one of its neighbouring voxels which makes the method fast compared to traditional simulation methods. The transition time of the jump from one voxel to another depends on the properties of the voxels, e.g. porosity and diffusion coefficient. Also the concentration isotherm of sorption can be taken into account in the simulations. [Sardini et. al., 2003; Voutilainen et. al., 2012]

In the TDD method it is presumed that information about the apparent diffusion coefficient and local porosities is available. Using this information, the transition probability for each jump between the voxels can be determined. In general, X-ray tomography has been used to obtain a 3D digital image of the sample being investigated with the TDD method. Linking 3D image data to the porosity data from ^{14}C PMMA method it is possible to model the diffusion of solutes in heterogeneous matrices. In practice, the TDD method describes the through-diffusion curve of nuclides in the heterogeneous rock matrix. [Voutilainen et. al., 2012]

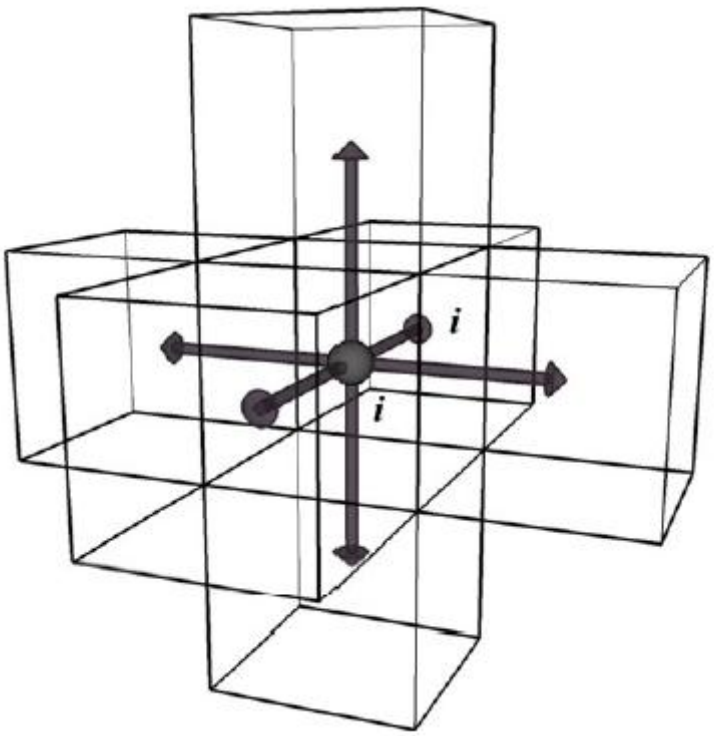

Fig 6.1. Illustration of the possible jumps in a 3D voxel. A particle in the image is forced to jump to one of the adjacent voxels and the transition time depends on the properties of the voxels. [Voutilainen et. al., 2012]

7. Analytical methods

7.1. Gamma counting

In this study, the gamma radiation (356 keV, 62 %) that the ^{133}Ba nucleus emits was measured with a solid scintillation detector to study the sorption and diffusion behaviour of barium [National Nuclear Data Center]. Gamma radiation is chargeless and very penetrating and thus produces only little ionisation in materials compared to alpha or beta radiation. As a consequence, scintillation or semiconductor diode detectors with high atomic numbers and high electron densities must be employed to maximize the interactions of the radiation and the detector material. The measurement of gamma radiation utilises the interaction mechanisms between the radiation and the material, of which photoelectric adsorption is most notable [Knoll, G.F., 2010].

The gamma radiation was measured with a crystalline sodium iodide detector, the function of which is dependent on the energy states in the crystal lattice of the detector

material. The electrons have only discrete energy bands in material, the valence band and the conduction band which represents the electrons having enough energy to migrate freely in the crystal lattice [Klemola, S., 2002]. Adsorption of energy can result in the elevation of an electron from the valence band to the conduction band leaving a hole in the valence band. By adding impurities in the crystal lattice, the return of the electron to the valence band becomes more energy efficient resulting in the emission of a visible photon [Knoll, G.F., 2010].

The scintillation crystal is optically connected with a photo cathode to which the photons emitted from the crystal are directed. The electrons generated in the photo cathode are accelerated with a series of electrodes, dynodes, where the amount of electrons is multiplied at every dynode. The current pulse that is acquired from the detector is first converted with a pre-amplifier into a voltage pulse, the height of which is proportional to the charge of the pulse [Klemola, S., 2002]. Furthermore, the voltage pulse is amplified and shaped with a linear amplifier after which the pulse is directed into an analog-to-digital converter (ADC) which sorts the pulses according to their height, that is, the gamma energy, to different channels of a multiple channel analyser [Knoll, G.F., 2010]. A schematic picture of a scintillation detector is presented in Fig 7.1.

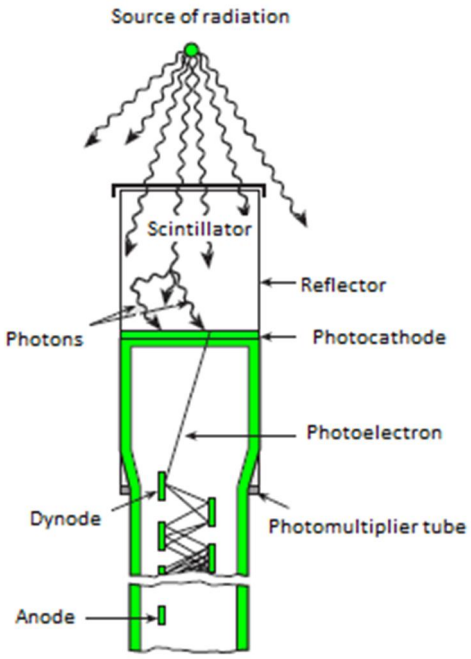

Fig 7.1. A schematic picture of a scintillation detector [Klemola, S., 2002].

7.2. Scanning electron microscopy and elemental analysis

The objective of microscopy techniques is to provide a magnified image with which features that are beyond the resolution of a human eye can observe. However, scanning electron microscopy (SEM) actually provides a contrast image of the electrons being scattered from the surface of the sample [Brundle, C.R. et al., 1992]. As a consequence it does not provide the same information that could be obtained by analysing the sample visually but it rather gives information about the topography and morphology of the sample. In addition, coupling the SEM with energy or wavelength dispersive X-ray analytics provides information about the elemental composition of the surface of the sample [Lyman, C.E. et al., 1990].

The physical basis of operation is that a source of electrons is focused in vacuum into a fine probe that is scattered on the surface of the sample. The electrons in the electron beam interact with the atoms on the surface of the sample resulting in the emission of electrons from the sample. A fraction of the electrons emitted from the surface can be collected with detectors. Furthermore, the output of the electrons can be used to modulate the brightness of a cathode ray tube (CRT) producing an image on the CRT where every point of the beam is focused on the sample and mapped directly to a corresponding point on the screen [Brundle, C.R. et al., 1992]. The x- and y-inputs are driven with the x- and y-voltages rastering the electron beam and, as a consequence, when the amplitude of the voltage applied to the x- and y-deflection amplifiers is reduced by a known factor while the CRT voltage is kept constant, the magnification will be increased by the same factor providing a full screen display [Lyman, C.E. et al., 1990]. A schematic picture of the operation of SEM is presented in Figure 7.2.

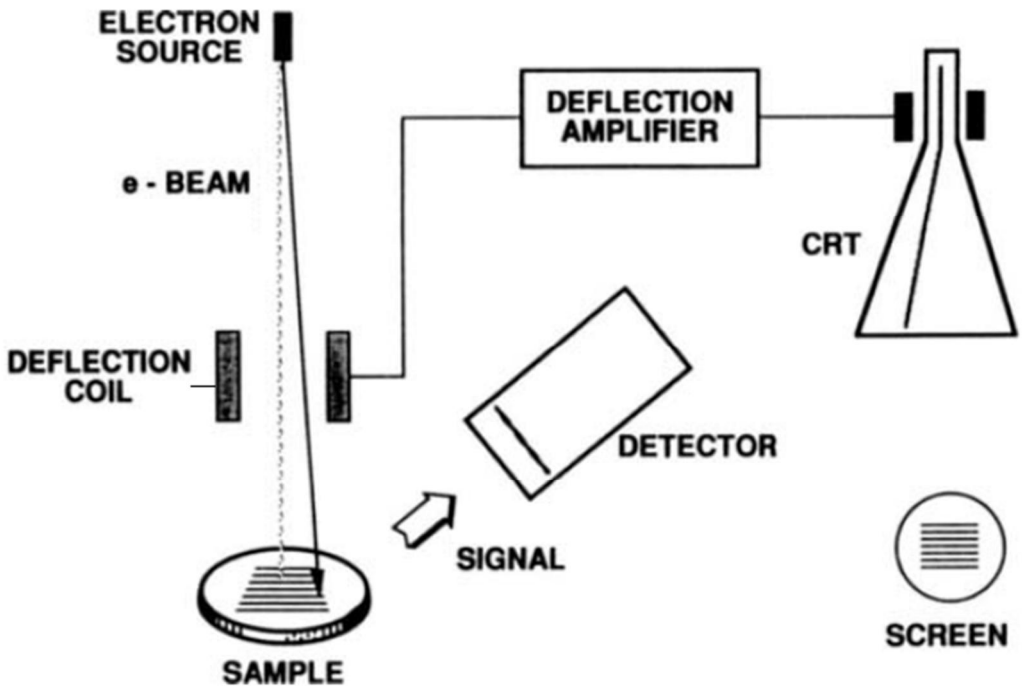

Figure 7.2. A schematic picture of the operation of scanning electron microscopy. [Brundle, C.R. et al, 1992]

There are three types of images produced in the SEM: secondary electron images, backscattered electron images and elemental X-ray maps. Secondary and backscattered images are produced by different mechanisms but they both are conventionally separated according to their apparent energies. When a high-energy electron interacts with an atom on the surface of the sample, it undergoes either an inelastic or elastic scattering with the atom. In an inelastic scattering some amount of energy is transferred to the other electron and if the energy transfer is fairly small, the emitted electron will not have enough energy to exit the surface [Brundle, C.R. et al., 1992]. As a consequence, if the energy transfer is more than the work function of the material, the electron emitted from the surface can exit the solid. The emitted electron is called a secondary electron (SE) when the energy of the emitted electron is less than 50 eV and most of such electrons are produced within the first few nanometers of the surface of the sample [Lyman, C.E. et al., 1990].

Higher than 50 eV energy electrons are primary electrons which have escaped the surface of the solid elastically without the loss of kinetic energy and they are conventionally referred to as backscattered electrons (BSE) [Lyman, C.E. et al., 1990]. However, many BSEs have energies that can be comparable to the energy of the primary electron beam. The backscattering is more likely to happen the higher the atomic number of the material in the analyzed area is. Thus a high-Z area will occur as a brighter image and the contrast is caused by elemental differences [Brundle, C.R. et al., 1992].

In addition, when the primary electrons in the SEM collide with the electrons of the sample, a core electron from an atom on the surface of the solid is ejected. The atom will be left in an excited state which decays to its ground state by emitting either characteristic X-ray photons or Auger electrons. The X-ray photons can be separated by their energy in an energy dispersive X-ray detector (EDS) or by wavelength with a wavelength spectrometer (EPMA) [Brundle, C.R. et al., 1992]. The X-ray photons are element-characteristic and they can be used to produce elemental maps of the sample which show the spatial distribution of different elements on the sample. The spatial resolution of an image based on the characteristic X-ray photons is rarely better than 0.5 μm since the primary electrons can travel long distances in the solid before losing enough energy to not to be able to excite X-ray emissions, which means that a large volume of the sample will produce X-rays for any position of the smaller primary beam [Lyman, C.E. et al., 1990].

Very little sample preparation is needed in SEM in imaging mode. For elemental analyses the sample needs to be polished as very even surfaces are needed. In addition, the sample needs to be vacuum compatible, conductive and it must fit the stage and specimen chamber of SEM. If the sample is not conductive enough, as often is the case with rock samples, the conductivity of the sample can be enhanced by coating the sample with a film of carbon or titanium [Goldstein, J.I. et al., 2012]. In such a case, care must be taken to avoid uneven coating which might lead to distortions in the image. Furthermore, when analysing the elemental composition of the sample with X-ray analysis, the X-ray peak of the coating material must be excluded in the analysis. If coating of the sample is not an option, uncoated insulating samples can be studied additionally with low primary beam voltages (<2 keV) but this results in the weakening of the image resolution to some extent. [Brundle, C.R. et al., 1992]

In an energy dispersive spectrometer, X-rays of all energies are detected by a detecting material, which is most commonly a lithium-drifted silicon crystal. EDS is able to detect all elements heavier than beryllium if present in the sample in sufficient quantity [Brundle, C.R. et al., 1992]. The minimum detection level for elements heavier than Z=11 has been found to be as low as 0.02 % weight but, in practice, it is about 0.1% weight because of high background and broad peaks. In addition, if severe overlap of peaks occurs, the minimum detection limit can be as high as 1-2 % weight. Furthermore, for light elements (Z<10) the minimum detectable limit is usually 1-2 % weight even under the best conditions [Friel, J.J., 2003].

The accuracy of quantitative analysis has been found to be above 2 % for major concentrations using well-polished standards with a composition similar to the sample. A value of 4-5 % can expected for general analysis using pure element standards and, in addition, the accuracy of analyses without standards will be much worse [Brundle, C.R. et al., 1992]. The concentration of the elements and the roughness of the surface of the sample will also affect the accuracy so that small concentrations and rough surfaces result in poor accuracies [Goldstein, J.I. et al., 2012].

One major advantage concerning EDS is that it can be positioned very close to the sample and thus present a large solid angle for the collection of the X-rays emitted from the surface of the sample. The solid angle in a typical energy dispersive X-ray detector configuration is about 10 times greater than that of a wavelength spectrometer [Brundle, C.R. et al., 1992]. In addition, with EDS more X-ray photons will be collected per incident electron, so that either a smaller probe diameter or lower beam current can be used which reduces specimen damage significantly. Furthermore, the electronics of EDS is fairly easy to interface to most instruments providing an only limitation of the need to cool the spectrometer with a large nitrogen cryostat [Friel, J.J., 2003].

In wavelength dispersive spectroscopy, on the other hand, an analyzing crystal is placed in front of the detector to screen out all X-rays but the desired wavelength. The exclusion of wavelengths is done by diffracting the X-rays through an analyzing crystal according to Bragg's law:

$$n\lambda = 2d \sin\theta \qquad 7.1.$$

where n is an integer number of wavelengths, λ is the wavelength, d is the known spacing between atom planes in a crystal and θ is the diffraction angle. In order to meet with the requirements of Bragg's law, the spectrometer must be moved throughout a range of angles and the crystal must remain in the focusing circle throughout its range of motion so that the location on the specimen from which X-rays are produced must be in X-ray focus [Goldstein, J.I. et al., 2012]. As a consequence, X-ray maps cannot be collected at magnifications of less than about 2000 times, because at lower magnifications the beam is moved out of X-ray focus [Friel, J.J., 2003].

The efficiency of wavelength dispersive spectrometers is commonly significantly weaker than that of energy dispersive spectrometers with values of roughly 30 % which is mainly due to the losses in the diffraction crystal. However, wavelength spectrometers have high peak/background ratios which result in a low minimum detectability limit, often as low as 0.01% [Friel, J.J., 2003]. As a result, much smaller concentrations can be detected with wavelength dispersive spectrometers than with energy dispersive [Goldstein, J.I. et al., 2012].

7.3. Autoradiography techniques

The radionuclide analysis of solid samples can be done by traditional counting methods, such as gamma counting. However, in traditional counting methods the sample needs to be homogenised before the analysis which destroys the information about the location of the radionuclides in x-y plane. Measuring radionuclides with imaging techniques, such as autoradiography techniques enables the preserving of the spatial location of the radionuclides as well as provide information about the intensity of the activity of the sample in centimetre scale [Upham, L.V. and Englert, D.F., 2003]. Thus, a two-dimensional analysis of a surface can be obtained via autoradiography techniques providing more data, for example, on the sorption processes of radionuclides onto different mineral surfaces.

7.3.1. Film autoradiography

Film autoradiography is a method of detecting alpha beta particles as well as gamma emission. However, autoradiography has been used mostly for the detection of beta particles although the best resolution is achieved by alpha particles. It is based on the reduction of silver ions to silver atoms within a film developing emulsion where the image to be developed is revealed by subsequent development of the film with the developing solution [Upham, L.V. and Englert, D.F., 2003]. This will result in the reduction of all of the silver atoms of an entire silver halide crystal grain to metallic silver producing an autoradiographic image of the radioactivity on the film [Boyd, G.A., 1955]. A single hit from a beta particle or gamma ray with a high enough energy can be sufficient to convert a grain to a developable state and the local blackening of film can be directly proportional to the intensity of the radiation that comes into contact with the film.

The inefficient transfer of emission energy from the radionuclides to the film limits the sensitivity of film autoradiography. Although very low detection limits have been observed (as low as 0.02 DPM/mm^2), measurements to achieve this level require exposure times of several months, depending on the radionuclide [Upham, L.V. and Englert, D.F.,

2003]. As a result, film autoradiography is best suited in terms of sensitivity for the detection of intermediate energy radionuclides such as ^{14}C and ^{35}S, which emit beta particles with energies of 156 keV and 167 keV, respectively. For beta particles with higher energy and gamma emissions the sensitivity is limited because they pass through the film and only a small portion of them is detected.

Concerning the source of radioactivity, there are several factors that govern the resolution of film autoradiography. Firstly, the choice of radionuclide is important because lower energy radionuclides emit particles with shorter path lengths in the film providing better resolution than higher energy radionuclides that travel further [Upham, L.V. and Englert, D.F., 2003]. Secondly, the distance between the source and the film emulsion affects the resolution so that the increased distance between sample and emulsion decreases resolution markedly [Schmidt, K.C. and Smith, C.B., 2005]. Lastly, samples that are thicker exhibit less resolution than thinner samples.

The most significant of all the factors affecting the resolution is the distance between the sample and the film [Upham, L.V. and Englert, D.F., 2003]. As a result, the sample should be placed as close as possible to the film to achieve the highest resolution. The second and third most important factors are the energy of the radionuclide, which should be at an intermediate level, and the thickness of the sample, which should be kept as thin as possible [Schmidt, K.C. and Smith, C.B., 2005].

A film autoradiogram presents the spatial activity distribution of a sample that can be determined by measuring the optical density of the film. There is a threshold level of activity for any given exposure time to cause a blackening of the film and concomitant measure of optical density. There is also a direct relationship for any given exposure and for a limited activity range, between the activity of a sample and the optical density of the film [Siitari-Kauppi, M., 2002]. The so-called linear dynamic range for any given film is between 1.5 and 3 magnitudes of activity [Upham, L.V. and Englert, D.F., 2003]. The level of activity at which the film is completely black or overexposed presents the upper

limit of detection for any given exposure and, furthermore, represents saturation of the silver halide grains of the film in that investigated area [Boyd, G.A., 1955].

There are several advantages associated with film autoradiography. It provides the best resolution for accurate localization of radioactivity on an investigated surface [Siitari-Kauppi, M., 2002]. The use of film also provides a permanent, unalterable record of the sample. Unlike digital imaging methods, film is a tangible and direct representation of the sample. Additionally, film autoradiography is the lowest cost alternative for radionuclide imaging despite the cost of developing chemicals and the overhead of maintenance of a darkroom.

In addition to advantages, some disadvantages remain in the utilisation of film autoradiography. The detection limit of activity may be low but the time needed to achieve these levels is very long (several months) and usually prohibitive [Upham, L.V. and Englert, D.F., 2003]. In addition, the linear dynamic range for film autoradiography is limited to two orders of magnitude of activity which makes the determination of the exposure time for any given sample difficult in order to achieve a successful autoradiogram. The exposure time needed to obtain a linear representation of all parts of the sample, is often difficult to estimate although the activity of the sample could be estimated. To quantify the activity using film autoradiography, the film must be scanned with an appropriate scanner, e.g. densitometer, or digitized with a CCD camera which makes the analysis more time consuming and weakens the resolution [Kämäräinen, E., et al., 2006]. Finally, reports of health effects, e.g. respiratory effects, have been documented in radiographers who process x-ray films. This suggests that the chemicals used in the developer solutions together with poor ventilation circumstances can have negative health effects.

Film autoradiography has been widely applied in the ^{14}C-polymethylmethacrylate (PMMA) impregnation method which can be used to investigate the pore structure and porosity of rock samples in a centimeter scale as well as the two dimensional porosity distribution of the connected pores [Hellmuth, K-H. et al., 1999]. In the method a rock

sample is first impregnated with ^{14}C-labelled MMA, after which the MMA is polymerized. A film is then exposed with the PMMA-sample and digitized. The amount of tracer in the sample can be determined from the blackening of film and the amount is proportional to the porosity of the sample which can be determined with a Mankeli program. Mankeli is a Matlab based program that defines the porosity of rock samples based on the information acquired from autoradiography [Siitari-Kauppi, M., 2002].

7.3.2. Digital autoradiography

Digital autoradiography imaging or storage phosphor screen imaging is a method in which phosphor screens, or ‘‘imaging plates’’ are used to trap the energy of the emissions of the radionuclides. In digital autoradiography radioactive samples are exposed to phosphor screens, which store energy in the photostimulable crystals ($BaFBr : Eu^{2+}$). The energy of the radionuclide ionizes Eu^{2+} to Eu^{3+} in the crystal, which liberates electrons from the valence band to the conduction band of the phosphor crystals [Knol, R.J.J. et al., 2008]. Furthermore, the electrons are trapped in bromine vacancies, which are introduced during the manufacturing process of the crystal. Exposure to red laser light (approximately 633 nm) releases the trapped electrons from the bromine vacancies back to the conduction band of the crystals, converting Eu^{3+} back to Eu^{2+}. This process releases photons at about 390 nm which are detected with a conventional high-quantum-efficiency photomultiplier tube. [Upham, L.V. and Englert, D.F., 2003]

There are several systems available for the scanning and creating an image of the radioactive samples exposed to the storage phosphor screen imaging system. For example, one mechanism is described as a modified drum scanner which has originally been a conventional densitometer used in the film autoradiography [Yonekura, Y. et al., 1983]. One drum in the system is used to scan the phosphor screen and the other to imprint the image onto normal photographic film. The rotation speed of the drum can be set manually or by the computer as the screen is scanned with a helium–neon laser (633 nm) and the light is collected by using a reflecting glass assembly and two PMTs with different sensitivities. Later systems were designed so that the imaging plate is moved on a conveyer belt mechanism and a stationary helium–neon laser is directed by a

galvanometer controlled mirror to sweep in the x direction across the screen [Upham, L.V. and Englert, D.F., 2003]. As a result, the light is collected by a light collection guide that moves in the y direction and focuses the light into a single photomultiplier tube.

Sensitivity of digital autoradiography can be described as the minimum detectable levels of activity or as the speed at which comparable levels of activity can be detected. For storage phosphor systems minimum detectable levels of activity of as low as 0.5 DPM/mm^2/h for ^{35}S and 0.1 DPM/mm^2/h for ^{32}P have been reported [Upham, L.V. and Englert, D.F., 2003]. Another commonly used measure for the detection threshold is signal-to-noise ratio used also in liquid scintillation counting [Yonekura, Y. et al., 1983]. However, in contrast to liquid scintillation counting, there is no relationship between the background fluctuation and the background itself in digital autoradiography. As a result, the fluctuation in the background must be calculated separately to measure the signal-to-noise ratio in digital autoradiography. The background values are arbitrarily set in the electronics in such a way that the values are never below zero. Consequently, the fluctuation in the noise can be measured and the sensitivity of any digital autoradiography system can be quantified.

The same factors involving the samples in film autoradiography affect the resolution also in digital autoradiography. However, characteristics of the storage phosphor system and the characteristics of the phosphor screens used to capture the images also affect the resolution in digital autoradiography. Thus, due to the mechanical differences between systems it is impossible to compare the resolution of each instrument independent of the variations between the types of phosphor screens [Upham, L.V. and Englert, D.F., 2003]. However, the resolution may be compared between selected instruments in terms of ^{14}C, keeping in mind that the characteristics of the screens used in the measurements, as well as the characteristics of the imaging systems, affect the resolution performance [Knol, R.J.J. et al., 2008].

The linear dynamic range in digital autoradiography imaging is substantially larger than that of film autoradiography since, typically, digital autoradiography can provide linear

data of four to five orders of magnitude [Labarre, P. et al., 1997]. The linear dynamic range is highly important in assessing the exposure time which needs to be estimated separately for each sample. A too short exposure time can result in nonlinear results for lower activity areas of the sample whereas a too long exposure time can result in the overexposure or saturation of the phosphor screen readout. Thus a longer linear dynamic range is a significant advantage which provides less chance of error the assessment of the exposure time [Upham, L.V. and Englert, D.F., 2003].

In contrast to film autoradiography, digital autoradiography provides quantitative data, the accuracy of which is dependent to some extent on the user technique since the phosphor screen is separate from the instrument and cannot be calibrated as such [Kämäräinen, E., et al., 2006]. For example, while scanning the phosphor screen some of the data on the phosphor crystals will be erased since exposing the screen to white light causes the crystals to be returned to ground state. As a consequence, in order to erase the image from the phosphor screens, they should be flooded with white light for 30 s to 5 min, depending on the screen type, for the de-excitation of the crystals to take place [Knol, R.J.J. et al., 2008]. Furthermore, phosphor screens are sensitive to cosmic radiation and they accumulate background while they are stored in the packaging [Upham, L.V. and Englert, D.F., 2003]. Due to this, they need to be erased before every exposure with a common fluorescent light box. Consequently, it is recommended that the lights in the lab are turned off while loading a phosphor screen into a scanning instrument in order to avoid the erasure of the data.

Digital autoradiography provides several advantages over film autoradiography for the quantification of radionuclides. It has been discovered that phosphor screens are about 250 times more sensitive than X-ray films for the detection of ^{32}P and about 60-100 times more sensitive for the detection of ^{14}C and ^{35}S. As a rule, a sample requiring a 30-day exposure with film autoradiography can be imaged and quantified in three days with digital autoradiography [Labarre, P. et al., 1997]. Additionally, the larger linear dynamic range associated with digital autoradiography provides a better linear representation for samples that may require two separate film exposures of different lengths of time [Kämäräinen, E., et al., 2006]. Furthermore, no hazardous chemicals are needed with

reusable storage phosphor screens in contrast to film autoradiography. Finally, the handling of several simultaneous exposures is less laborious with digital autoradiography due to the short scanning times.

Additionally, there are a few disadvantages regarding the digital autoradiography imaging method. In contrast to film autoradiography, the only permanent record of the sample is the electronic file and a possible printout of the file. Furthermore, incomplete erasure of the exposed image or mishandling of the phosphor screen can result in ”ghost images” affected by the previous exposures [Upham, L.V. and Englert, D.F., 2003]. In film autoradiography each film is disposable and thus not affected by previous exposures. Other challenges with digital autoradiography are caused by the signal fading of the phosphor screens, lack of individual calibration, the need to clean the screens every once in a while, sensitivity to light which requires working in subdued lighting, the need to erase the screens before exposure to avoid background effects and the challenge of choosing the correct exposure time. These challenges are independent of the scanning system and can significantly affect the results from the scanning which can be expected for quantitative radionuclide analysis.

The PMMA method described earlier can additionally be performed using digital autoradiography [Sardini, P. et al., 2015]. In addition, digital autoradiography has been used to investigate tritium traces on concrete structures of a laboratory under dismantling process [Fichet, P. et al., 2012]. Furthermore, digital autoradiography has been employed in the TLC-analyses used in the development of the synthesis of radiopharmaceuticals [Kämäräinen, E-L. et al., 2006].

8. Experimental research

8.1. Introduction

In this study the distribution coefficients of barium in pegmatite, veined gneiss, granodiorite and their main minerals were obtained by batch sorption experiments carried out as a function of the concentration of barium. The distribution coefficients of biotite were modelled with the PHREEQC calculation code. The results of different rocks and minerals were compared with each other and the sorption mechanisms onto different mineral surfaces were evaluated. The sorption results of barium were also compared with sorption results obtained from a previous study for caesium. In addition, the diffusion of barium into the rock cubes was also studied both experimentally and computationally. Finally, the rock cubes from the diffusion experiments were studied with autoradiography and scanning electron microscopy.

8.2. Minerals and rocks

The minerals used in this study were quartz, plagioclase, potassium feldspar and biotite. Additionally, granodiorite from the Grimsel test site and veined gneiss and pegmatite from the Olkiluoto site were studied. The samples for the batch sorption experiments were crushed by milling and sieved and the grain size used in the experiments was <0.3 mm. The purity of the minerals was controlled by characterizing them with the XRD method in the Geological Survey of Finland. In addition, the specific surface areas of the minerals were determined at Chalmers University with Kr-BET using a gas adsorption analyzing instrument (Micromeritics ASAP2020). Rock cubes acquired from the test sites were also studied and the roughness of their surfaces was investigated with SEM.

It was discovered in the XRD experiments that the quartz used in the sorption experiments was 95 % pure SiO_2 with two minor unidentified phases. It was concluded with the aid of scanning electron microscopy that the unidentified phases were most probably compounds containing K-Cl and Fe-Ti-(Ca)-Si-O but the identification was indefinite as the concentration of the compounds was so small. Additionally, the biotite sample was 80 % biotite and 20 % chlorite and the biotite was discovered to be phlogopite, the magnesium rich end member of the biotite solid solution series. The potassium feldspar

sample was found to be the most stable polymorph of potassium feldspar, maximum low microcline, with inclusions of albite (10 %). Additionally, the plagioclase was revealed to have numerous impurities, such as inclusions and mixed grains with the composition of plagioclase (90%), pyroxene (5%), quartz (3%), biotite (1 %) and chlorite (1 %). The plagioclase was optically purified with the aid of microscopy in the Geological Survey of Finland.

The mineral compositions of the veined gneiss and pegmatite used in the experiments were found to resemble the compositions presented in Table 4.1. and Table 4.2. The veined gneiss sample studied consisted of quartz (20 %), plagioclase (15 %), potassium feldspar (10 %) and mica (50 %). The mica content of veined gneiss was higher than typically (20±15 %). The pegmatite sample, on the other hand, consisted of quartz (15 %), plagioclase (30 %), potassium feldspar (40 %) and mica (5 %). Inclusions of chlorite, cordierite and sillimanite were also found in both rocks but their abundancy did not exceed 5 %. Additionally, the granodiorite was consisted of plagioclase (40 %), quartz (30 %), potassium feldspar (20%) and biotite (5 %).

The specific surface area of the sieved samples (<0.3 mm) was measured in the Chalmers University of Technology. The magnitudes of the specific surface areas of the minerals were quartz (0.32 m^2/g) < plagioclase (0.60 m^2/g) and potassium feldspar (0.66 m^2/g) < biotite (4.57 m^2/g). In addition, the specific surface area of the crushed granodiorite was 0.33 m^2/g, and the specific surface area of the crushed veined gneiss was 1.48 m^2/g and of the pegmatite 0.34 m^2/g. The differences in the surface areas are caused by the different mineralogical structures. Veined gneiss is consisted of abundant layered biotite zones which make up a lot of surface area whereas the granodiorite and pegmatite mostly consist of quartz and feldspars, which are more grained providing less specific surface area than the layers. In addition, the sawing process increased the specific surface area by giving rough edges to the surface of the rock cubes, which is a typical phenomenon occurring in the sawing of the rock. Scanning electron microscope pictures of the structures of veined gneiss, granodiorite and pegmatite are presented in Figure 8.1. It can be seen in the FE-SEM image of pegmatite that it suffered from the sawing process leaving it rough, brittle and with fissures of tens of micrometers wide.

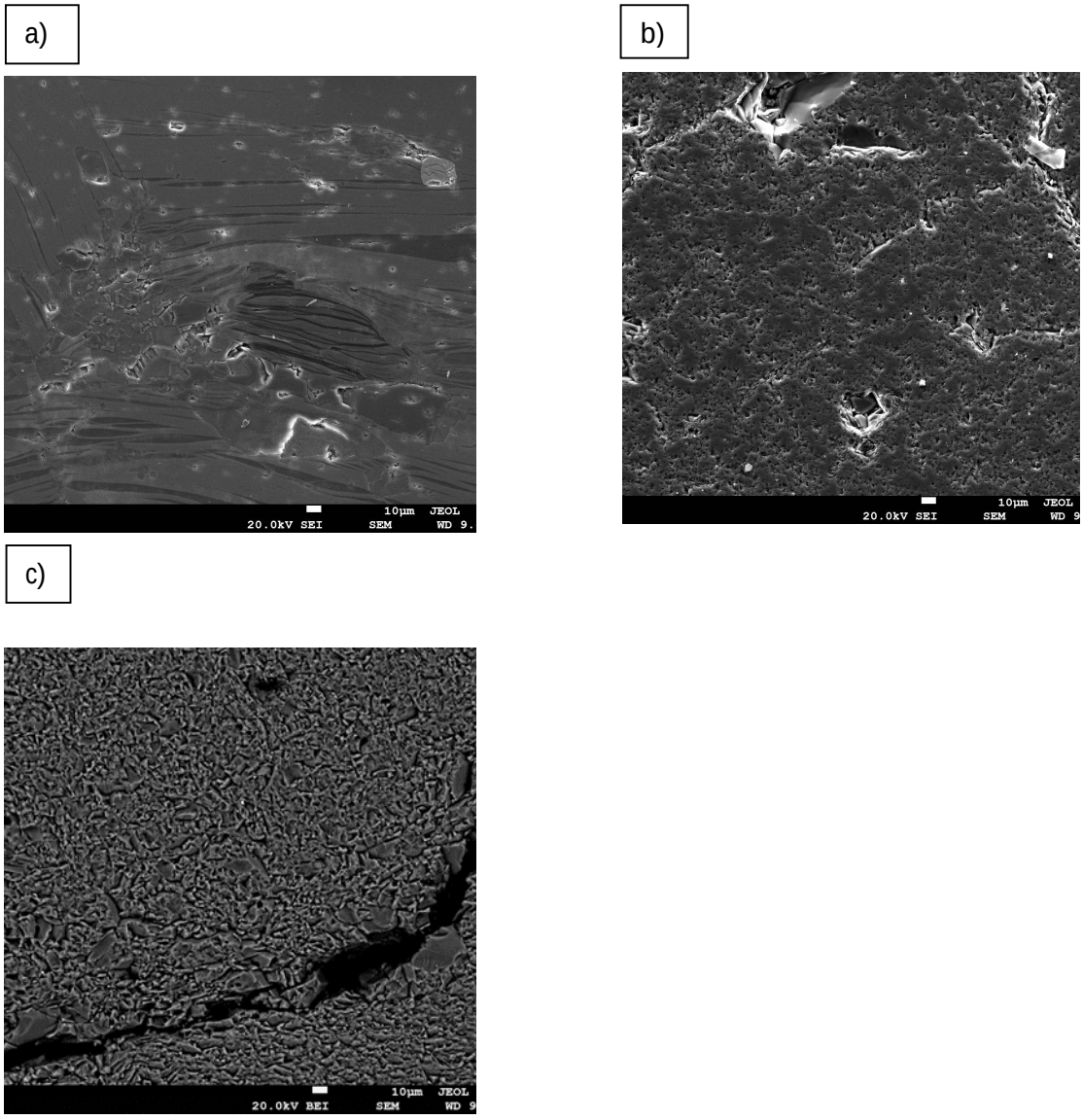

Figure 8.1. The FE-SEM images of the sawn surface of a) veined gneiss, b) granodiorite and c) pegmatite. The effect of sawing on the surface can be seen especially on pegmatite and granodiorite whereas the surface of veined gneiss is polished more properly.

8.3. Groundwater simulants

8.3.1. Grimsel groundwater simulant

The groundwater in the Grimsel test site is significantly alkaline and weakly saline with low ionic strength and, thus, few competing ions for barium [Mäder, U.K. et al., 2006]. The chemical composition of the groundwater simulant used in the experiments was

performed based on the fracture water data from the Grimsel site [Mäder, U.K. et. al, 2006] and it is summarized in Table 8.1

Table 8.1. The chemical composition of the Grimsel groundwater simulant [Schatz, T. et al., 2013].

Component	Molality
pH	9.7
Na^+	$6.9 \cdot 10^{-4}$
K^+	$5.0 \cdot 10^{-6}$
Ca^{2+}	$1.4 \cdot 10^{-4}$
Mg^{2+}	$6.2 \cdot 10^{-7}$
HCO_3^-	$4.5 \cdot 10^{-4}$
Cl^-	$1.6 \cdot 10^{-4}$
S	$6.1 \cdot 10^{-5}$
Br^-	$3.8 \cdot 10^{-7}$
F^-	$3.6 \cdot 10^{-4}$
[Si]tot	$2.5 \cdot 10^{-4}$
[Fe]tot	$3.0 \cdot 10^{-9}$
[Mn]tot	$5.0 \cdot 10^{-9}$

8.3.2. Olkiluoto groundwater simulant

The fracture groundwater in the Olkiluoto site is slightly basic with the pH values ranging from 7.3-8.0 and it is mainly of Na-Cl type. Additionally, the groundwater is brackish with maximum chloride content of 600 mg/l at the depths from 40 m to 500 m. However, some fracture waters from the area have been noticed to have a maximum chloride content of up to 5 g/l. Hydrological mixing experiments have been conducted and it has been discovered that the groundwater contains seawater that resembles the present water in the Baltic Sea. The chemical composition of the Olkiluoto groundwater simulant used in the experiments was performed based on the fracture water data from the Olkiluoto site and it is presented in Table 8.2.

Table 8.2. The chemical composition of the Olkiluoto groundwater simulant [Huitti, T. et al., 1998].

Component	Molality
pH	6.9
Na^+	$1.2 \cdot 10^{-1}$
K^+	$2.0 \cdot 10^{-4}$
Mg^{2+}	$1.4 \cdot 10^{-3}$
Sr^{2+}	$5.7 \cdot 10^{-6}$
Ca^{2+}	$1.3 \cdot 10^{-2}$
Cl^-	$1.4 \cdot 10^{-1}$
Br^-	$4.1 \cdot 10^{-4}$
F^-	$7.9 \cdot 10^{-5}$
S	$3.1 \cdot 10^{-6}$
HCO_3^-	$2.0 \cdot 10^{-4}$

8.4. Batch sorption experiments

In this work the sorption of barium onto quartz, potassium feldspar, plagioclase, biotite, veined gneiss, pegmatite and granodiorite was investigated in a concentration range of barium from $1.0 \cdot 10^{-9}$ M to $1.0 \cdot 10^{-3}$ M. The concentration range was chosen for the experiments on the base of previous experiments. All experiments were conducted at room temperature and in the groundwater simulants described in Tables 8.1. and 8.2.

Crushed mineral and rock samples with grain size of <0.3 mm were first equilibrated with the groundwater simulant in liquid scintillation vials (20 ml) with a solid to solution ratio of 50 g/L after which the vials were agitated for two weeks. Such a large solid solution ratio was chosen to simulate the conditions of the in-situ diffusion experiments in Olkiluoto site where 250 ml of water is circulated in a borehole that is 1 m in length and 1 mm in width and in Grimsel site where 3 litres of water is circulated in a borehole that is 70 cm in length and 1 mm in width. The investigated concentration of barium was added to the samples with a nonradioactive barium salt ($BaCl_2$, Sigma-Aldrich) and a radiotracer of ^{133}Ba ($BaCl_2$ in 0.1 M HCl, Eckert & Ziegler) after which they were again agitated for two weeks for the ion exchange process to take place. The amount of the

added radiotracer of barium was 620 Bq / 10 ml (carrier $1.30 \cdot 10^{-9}$ g/l). The pH of the solutions was measured before and after the equilibration.

The samples were centrifuged (15 min, 4000 rpm with Sigma 3-16 KL) after the equilibration and the supernatant was pipetted to liquid scintillation vials. ^{133}Ba was measured from the supernatant with a Perkin Elmer automatic 1480 WIZARD 3'' gamma counter with a 20 min counting period. The distribution coefficients K_d of barium in the investigated minerals and rock samples were calculated from the percentages of barium sorption acquired from the relative activities of the measurements:

$$K_d = \frac{(A_{init} - A_{eq})}{A_{eq}} \cdot \frac{V}{m} \qquad 8.1.$$

where A_{init} is the initial activity of the tracer, A_{eq} is the equilibrium concentration of the radionuclide in the solution, V is the volume of the liquid phase and m is the mass of the solid phase. The sorption isotherms acquired from the experiments are to be employed in the heterogeneous diffusion modelling conducted with TDD.

8.5. Diffusion experiments with rock cubes

The rock cubes cored from Olkiluoto and Grimsel sites were first sawed to approximately 1 cm x 1 cm x 1 cm cubes. The cubes were equilibrated with the groundwater simulant (15 ml) for two weeks after which the radiotracer of ^{133}Ba (4600 Bq / 15 ml) and stable barium as $BaCl_2$ ($1 \cdot 10^{-6}$ M) was added. A schematic picture of the experimental setup used in the model is presented in Fig 8.2. The concentration depletion of tracer in the solution was monitored two times a day in the first week of the experiment and after that once a week by pipetting 10 ml of the solution and measuring the activity of ^{133}Ba with gamma spectrometry after which the solution was pipetted back to the vessel containing the rock cube. The decrease in the tracer concentration was monitored for six months. After the diffusion experiments were terminated, the rock cubes were sawed to thin layers, polished and studied with autoradiography and scanning electron microscope.

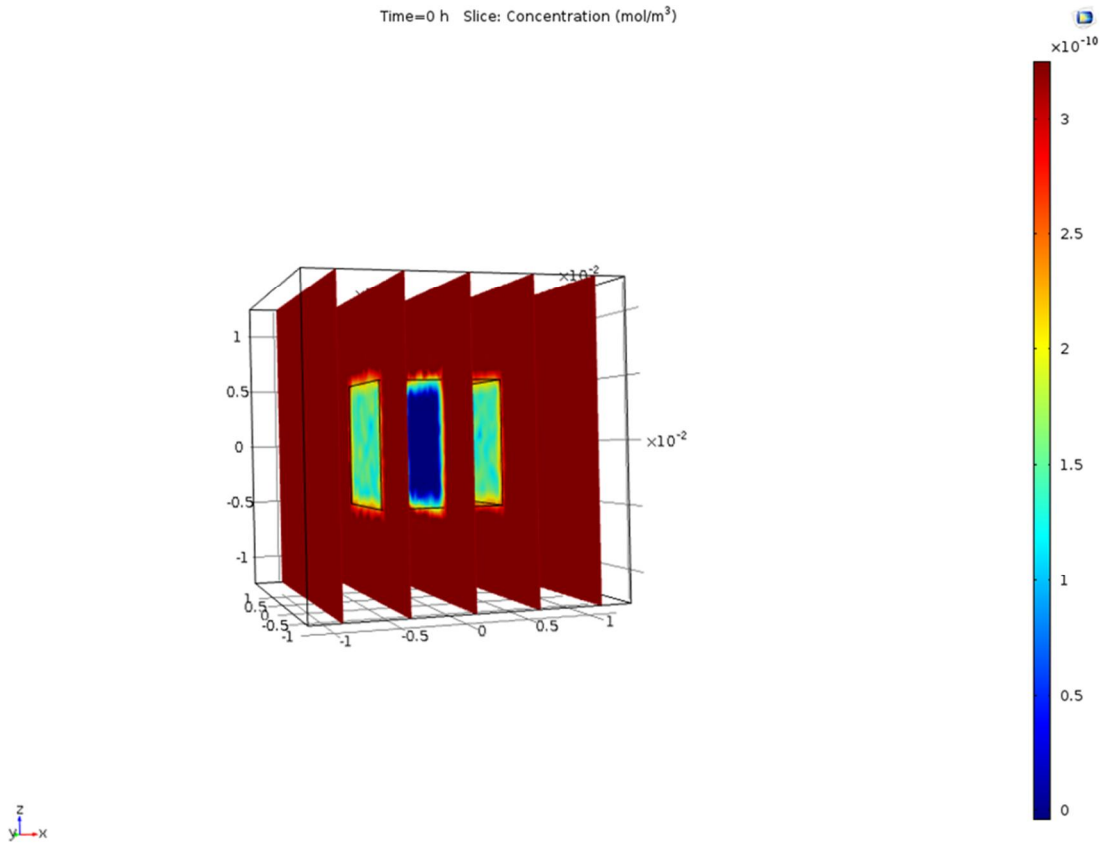

Fig 9.9. A schematic picture of the experimental setup used in the model at t = 0 h. The outer box represents the vessel containing the tracer solution and the inner box the rock cube.

8.6. Spatial activity distribution with autoradiography

The rock cubes employed in the diffusion experiments were sawed to thin layers (about 1 mm in thickness). Ethanol was used as a cooling agent in the sawing process to avoid the detachment of the sorbed barium from the surface in the process. The radioactivity of rock slices were exposed on both imaging plates and X-ray films to study the distribution of the sorbed barium in different minerals.

The samples were placed into an exposure cassette on a phosphor screen (Fuji Imaging Plate BAS-TR2025, Fuji Photo Film Co., Ltd., Tokyo, Japan) for the digital

autoradiography and the screens were exposed for one day. Lead sheets were carefully set on the samples to ensure proper contact between the phosphor screen and the film. After the exposure, the rock samples were removed from the phosphor screen in reduced lightning and the screen was scanned with a Fuji Analyzer BAS-1800 at 10 μm resolution. The obtained images were stored as digital files and later analysed and edited with image analysis programs Aida 4.0 (Raytest Isotopenmessgeräte GmbH, Straubenhardt, Germany) and the Corel Paintshop Pro X7 editing programme.

After the digital autoradiography, the samples were exposed on film for film autoradiography. The samples were set on a film (Kodak X Omat MA film, Kodak-Pathé, Paris, France) in a dark room and the film was carefully shielded from light. Lead sheets were carefully set on the samples to ensure proper contact between the samples and the film. The film was exposed for three days after which the samples were removed from the film in a dark room. The films were developed in a dark room by first keeping the film in a developer solution (AGFA Developer G 153 part A) for four minutes. The film was then rinsed under running water for 30 seconds after which the film was kept in a fixer solution (AGFA Developer G 153 part B) in the dark for four minutes and with lights on for six minutes. The film was then rinsed under running water for ten minutes after which the film was let dry for a day. Lastly, the film was digitized with a table scanner (CanoScan 9900F, Canon, optical resolution 2400 dpi) and the images were then edited with the Corel Paintshop Pro X7 editing programme.

8.7. Morphology and elemental analysis with scanning electron microscopy

The rock slices studied with autoradiography were additionally studied with field emission scanning electron microscopy in the Geological Survey of Finland. The samples were polished with diamond powder carefully on a glass platter to avoid the breaking of the samples. Especially the pegmatite samples were so brittle that they had a tendency to be fragmented. The samples were glued on sheet glass to make the handling of the samples easier after which they were coated with carbon.

After the preparation of the samples, they were studied with the Jeol JSM-7100F Schotky FE-SEM equipment having a high resolution option at the Finnish Geosciences Research

Laboratory (SGL). The FE-SEM was equipped with an Oxford Instruments EDS system of a X-mas 80 mm^2 silicon drift detector (SDD). The EDS system enables simultaneous imaging and analysis and superb analytical resolution (< 10 nm). In addition, the apparatus was equipped with INCAEnergy, INCAMineral and AZtecEnergy softwares, of which AZtecEnergy was used for X-ray mapping and image montage.

The morphology of the samples was first studied with a secondary ion beam to see the differences in the rock structures presented in Figure 8.1. After that the backscattering electrode was enabled and the distribution of different elements was analysed in two dimensions with the AZtecc software. The software allowed the mapping of large surface areas to find the sorbed barium. After the mapping, the maps were corrected with the TruMap option, which eliminated artefacts, corrected element overlaps and pulse pile-up and removed false variations due to X-ray background. The voltage used was 20 keV and the probe current was 9 μA.

8.8. Modelling

8.8.1. Ion exchange modelling with PHREEQC

The three site ion exchange model described earlier was performed with the PHREEQC program assuming that all aqueous species are in thermodynamic equilibrium. Firstly, the chemical composition of the groundwater simulants was identified in the SOLUTION keyword as given in Tables 8.1. and 8.2. Secondly, the different sorption sites were identified under the EXCHANGE_MASTER_SPECIES keyword and the corresponding exchange reactions under the EXCHANGE_SPECIES keyword. The selectivity coefficient *logK* values for the model were taken from the WATEQ4F.dat thermodynamic database, the values of which can be used to model solutions with a total ionic strength of < 0.5 M due to the limitations of the extended Debye-Hückel equation that has been used to calculate the aqueous activity coefficients [Fuller, A.J. et al., 2014]. In addition, the values for the selectivity coefficients for the exchange of barium were treated as fitting parameters in the model. The EXCHANGE keyword was used to define the composition and amount of the exchangers. Under the keyword the exchange formula designated the stoichiometry of the exchange species and the exchange sites. The number of the exchange sites was again treated as a fitting parameter.

Additionally, the SELECTED_OUTPUT keyword was used to produce a file from the output of PHREEQC suitable for processing by a data-management software, such as Excel. Under the keyword, the exchange assemblage was printed after the completion of the calculation. Furthermore, USER_PUNCH keyword was used to define a Basic program to print the distribution coefficients of barium in the selected-output file. USER_PUNCH allows the calculations of selected results to the selected-output file as the program is running to plot the desired data directly. The Lawrence Livermore National Laboratory database (llnl.dat, thermo.com.V8.R6.230) was used in the modelling to supplement the selectivity coefficients in the model.

8.8.2. Diffusion modelling with PHREEQC

PHREEQC was used to model the diffusion of barium into rock cubes in conjunction with sorption. However, PHREEQC is only capable of modelling 1D transport which made the model very simplified. Advection and dispersion, diffusion and diffusion into stagnant zones adjacent to the 1D flow system can be modelled under the keyword [Parkhurst, D.L. and Appelo, C.A.J, 1999]. The diffusion model used in this study was constructed by combining the ion exchange model with the TRANSPORT keyword.

Under the TRANSPORT keyword, the number of cells and the length of cells must be determined. In addition, the time step and the number of shifts or diffusion periods must be indicated. The number of shifts thus indicates the number of times the solution in each cell is shifted to the next cell and the total simulation time is *shifts x time step* where the time step defines the time that each diffusion period is simulated. In this study the total simulation time was equal to the time of the laboratory experiments, which was six months. In addition, it was defined in the flow direction that only diffusion occurs and that dispersivity of each cell was zero. The boundary conditions of the diffusion model was set to be closed, so that there is no flux at the boundary. This can be stated as the Neumann boundary condition, $\frac{\partial C(x_{end},t)}{\partial x} = 0$ [Parkhurst, D.L. and Appelo, C.A.J, 1999]. Lastly, the punch frequency was identified to select the shifts for which results were written to the selected-output file. To fit the data to the experimental data, the sorption parameters and the effective diffusion coefficient were treated as fitting parameters.

8.8.3. Diffusion modelling with COMSOL

The diffusion model obtained with COMSOL is much more complex than the one obtained with PHREEQC due to the 3D nature of the model. When COMSOL Multiphysics is solving the constructed models, it uses the *finite element method (FEM)*, in which the software runs the finite element analysis together with adaptive meshing and error control using a variety of numerical solvers which requires fairly considerably the random-access memory (RAM) of the computer [Comsol, 2012].

The diffusion model was constructed by first defining the geometry of the rock cube and the vessel containing the rock cube and the solution after which the materials for the water and the rock needed to be defined. The rock cube was assumed to be homogeneous. Transport of diluted species in porous media was chosen as the physics taking into account only the diffusion and adsorption. The barium concentration in the rock cube was defined as zero and the starting concentration was set for the vessel containing the liquid and the flux at the surface of the vessel was defined as zero. The objects were meshed on a fine grid to ensure the precision of the model. However, fine grid mesh made the simulation significantly slower.

A time dependent study case was selected and the simulation time was set to equal the time of the experiment. Additionally, the distribution and diffusion coefficients were treated as fitting parameters in the model. Lastly, the concentration decrease of the tracer in the vessel was studied with the cut line function.

9. Results and discussion

9.1. Distribution coefficients

9.1.1. Quartz

It was discovered in the sorption experiments that the sorption of barium on quartz was very small in all studied concentrations and in both studied groundwater simulants with distribution coefficient values of $1 \cdot 10^{-3}$ m^3/kg in magnitude (Fig 9.1.). In addition, the variation of the results was large which led to large uncertainties making the interpretation of the results difficult and a minor decreasing trend could be seen. The large uncertainties may be due to resilient solid phase in the measured liquid phase. Furthermore, the distribution coefficient values in Olkiluoto and Grimsel groundwater simulants were very similar within the uncertainty units of the results.

The small distribution coefficients obtained for quartz may be due to the preference of ion exchange over surface complexation as a sorption mechanism for the divalent cation Ba^{2+}. Ion exchange is not occurring and only weak surface complexation which can be seen as the small results for sorption. Additionally, it has been discovered in previous studies that quartz is not a strong adsorbent for divalent cations and that barium, strontium and cadmium will migrate through silica-rich geological environments at essentially the same rate as the flowing groundwater [Hayes, P.L. et al., 2008].

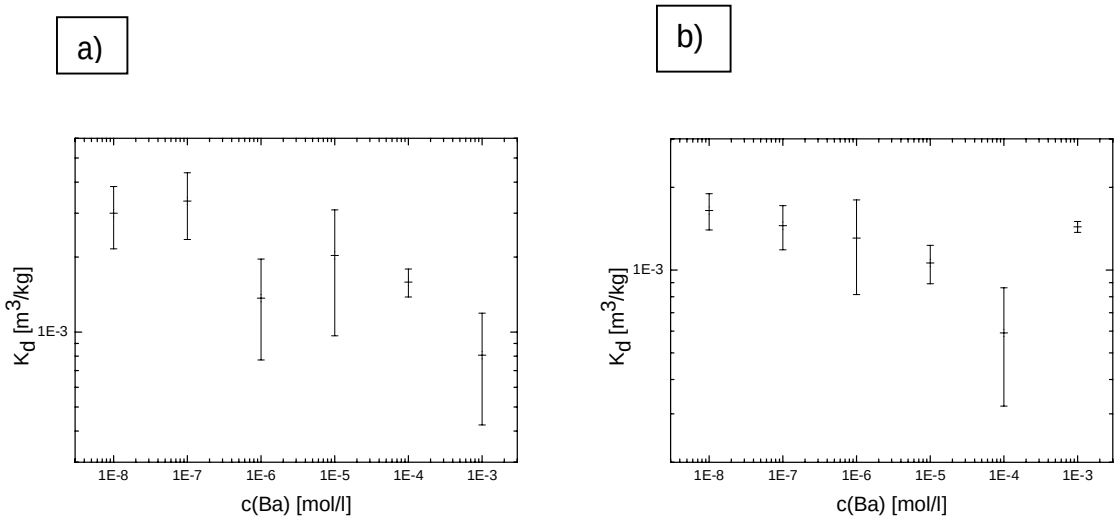

Fig 9.1. The distribution coefficients of barium on quartz as a function of barium concentration in the presence of a) Olkiluoto groundwater simulant at pH 6.5 and b) Grimsel groundwater simulant at pH 8.0. All data points represent the average of triplicate samples and the uncertainties are given as the standard deviation of the mean.

9.1.2. Plagioclase

On the contrary to quartz, the distribution coefficient results of barium on plagioclase showed a clear trend of decreasing as the concentration of barium was increased. However, the decrease was not linear but instead the values were roughly constant at low concentrations and the decrease started at concentrations of approximately 1·10-6 mol/L. The three site sorption model suggested for mica and clay minerals accounting for the saturation of specific sorption sites and the decrease of distribution coefficients in larger concentrations [Fuller, A.J. et al., 2014] cannot be used to explain the sorption behaviour in tectosilicates due to the lack of sheeted structure.

The sorption behaviour of barium on plagioclase was similar in both groundwater simulants but a difference in the magnitude of the results was observed (Fig 9.2.). The distribution coefficient values were 0.0089±0.0007 m^3/kg in $1 \cdot 10^{-7}$ mol/L in the Olkiluoto groundwater simulant whereas the values in the Grimsel groundwater simulant were 0.244±0.026 m^3/kg in $1 \cdot 10^{-7}$ mol/L (Table 9.2.). The difference is most probably caused by the larger concentration of competing ions for the sorption in the Olkiluoto groundwater simulant than in the Grimsel groundwater simulant. For instance, the molality of Ca^{2+} ions was $1.3 \cdot 10^{-2}$ mol/kg in the Olkiluoto groundwater simulant and $1.4 \cdot 10^{-4}$ mol/kg in the Grimsel groundwater simulant. The ion radius and charge of Ca^{2+} is similar to Ba^{2+}, which suggests that they compete for the same sorption sites on the surface of the minerals.

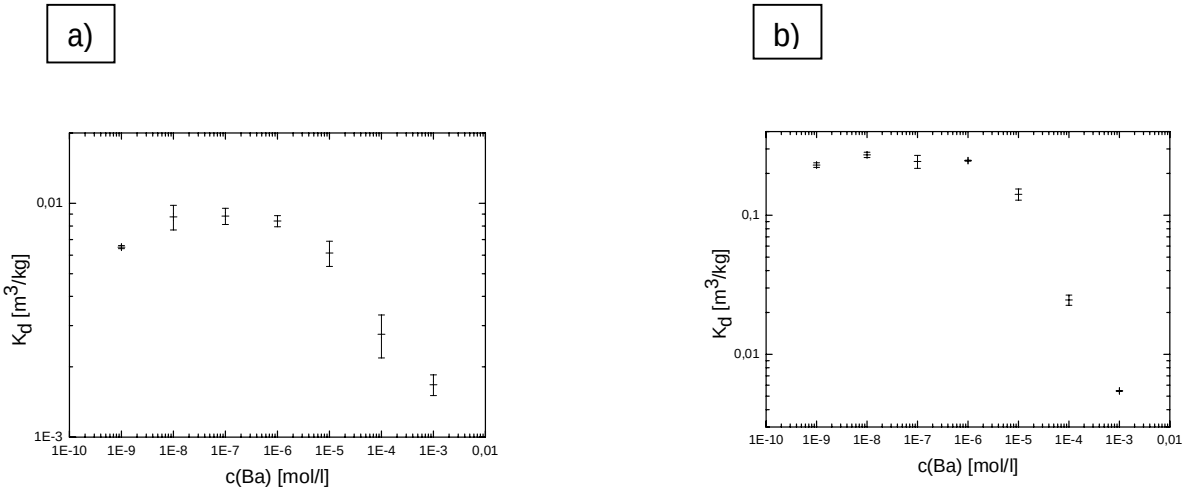

Fig 9.2. The distribution coefficients of barium on plagioclase as a function of barium concentration in the presence of a) Olkiluoto groundwater simulant at pH 8.7 and b) Grimsel groundwater simulant at pH 8.6. All data points represent the average of triplicate samples and the uncertainties are given as the standard deviation of the mean.

9.1.3. Potassium feldspar

The trend of the distribution coefficients of barium on potassium feldspar was similar to the results on plagioclase (Fig 9.3.). However, the distribution coefficients of barium were slightly smaller on potassium feldspar with values of 0.0032±0.0001 m^3/kg in $1 \cdot 10^{-7}$ mol/L in the Olkiluoto groundwater simulant and 0.140±0.001 m^3/kg in $1 \cdot 10^{-7}$ mol/L in the Grimsel groundwater simulant (Table 9.2.). Additionally, the same trend of the smaller distribution coefficients in the Olkiluoto groundwater simulant compared to the Grimsel groundwater simulant could be seen with potassium feldspar as with plagioclase. This reinforces the assumption of the role of competing ions for sorption in the more saline Olkiluoto groundwater simulant.

The slightly smaller distribution coefficients of barium on potassium feldspar than on plagioclase could be due to more preferential ion exchange sites in plagioclase. The plagioclase used in the experiments was rich in calcium whereas the potassium feldspar contained only little calcium. In addition, the potassium feldspar was microcline, which is the most stable polymorph of the potassium rich alkali feldspar [Klein, C. and Dutrow, B, 2007]. The structure is thermodynamically very stable and thus only little ion exchange occurs from the crystal structure.

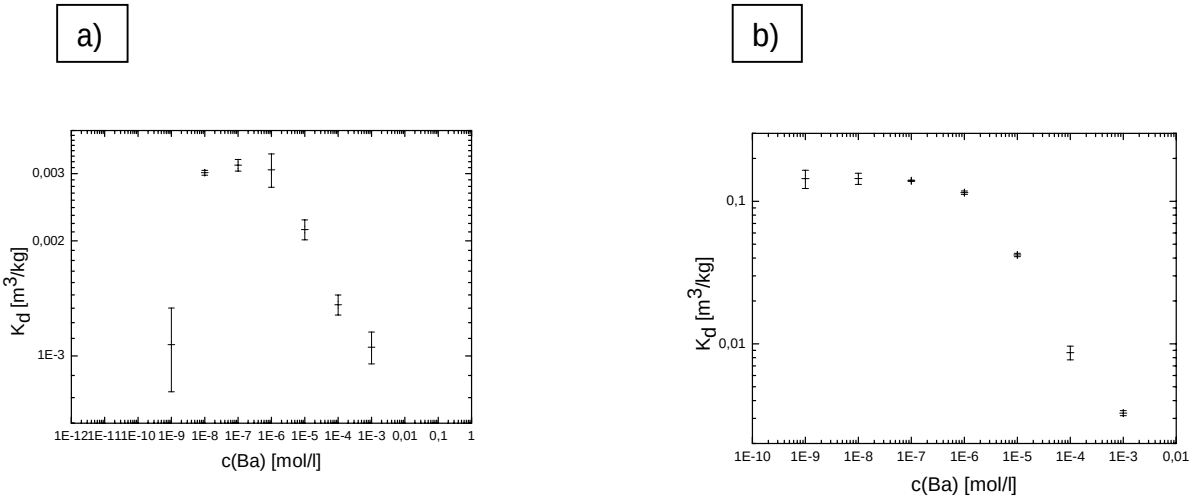

Fig 9.3. The distribution coefficients of barium on potassium feldspar as a function of the barium concentration in the presence of a) Olkiluoto groundwater simulant at pH 7.0 and b) Grimsel groundwater simulant at pH 8.1. All data points represent the average of triplicate samples and the uncertainties are given as the standard deviation of the mean.

9.1.4. Biotite

Of all the investigated minerals, the distribution coefficients of barium were largest on biotite with values of 0.084±0.001 m^3/kg in 10^{-7} M in the Olkiluoto groundwater simulant and 0.286±0.053 m^3/kg in 10^{-7} M in the Grimsel groundwater simulant (Table 9.2.). In addition, the magnitude of the distribution coefficients of barium on biotite was similar as on plagioclase (0.244±0.026 m^3/kg in the Olkiluoto groundwater simulant). In addition, similar trend as with plagioclase and potassium feldspar can be seen in the results as a function of barium concentration (Fig 9.4.). The distribution coefficients of barium on biotite were also modelled with PHREEQC and the model results are presented as the curve in Fug 9.4.

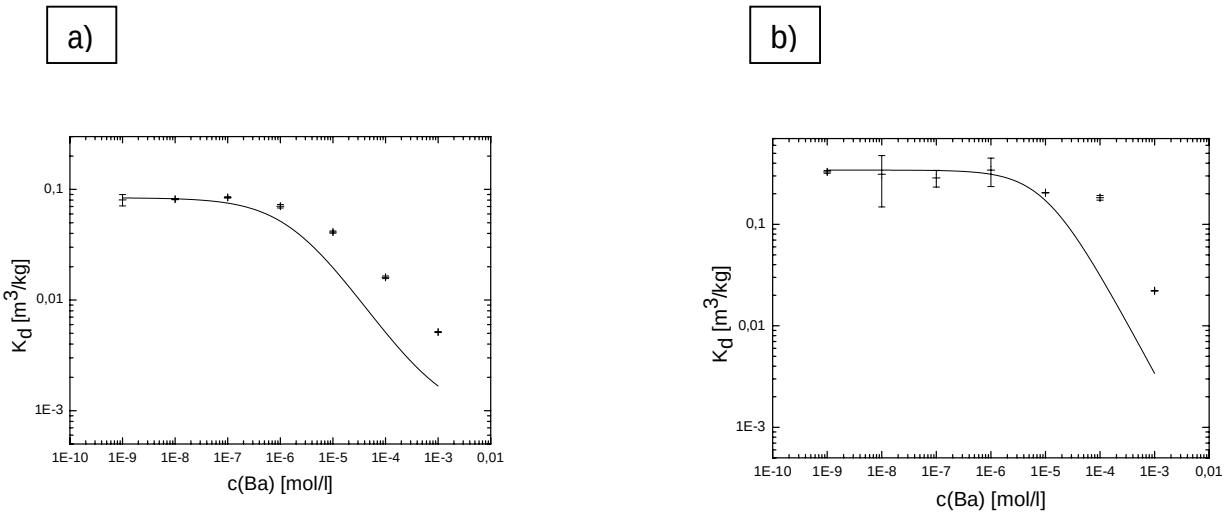

Fig 9.4. The distribution coefficients of barium on biotite as a function of barium concentration in the presence of a) Olkiluoto groundwater simulant at pH 8.3 and b) Grimsel groundwater simulant at pH 8.6. All data points represent the average of triplicate samples and the uncertainties are given as the standard deviation of the mean. The curves represent the modelled data.

The large sorption on biotite can be explained with the structure of the mineral. Biotite is consisted of layers that are connected with weak hydrogen bonds and the potassium ions are placed mainly in the interlayer sites of the mineral. The edges of layers of the mineral offer a lot of surface area for the sorption to occur, which could be seen from the specific surface areas determined with the BET method. In addition, the large surface area constituted of the layered structure of the biotite can be seen in Figure 9.5. where the upper part of the right picture shows the basal plane of the mineral structure offering only little surface area. The edges of the sheets, on the other hand, provide roughness to the surface adding to the specific surface area.

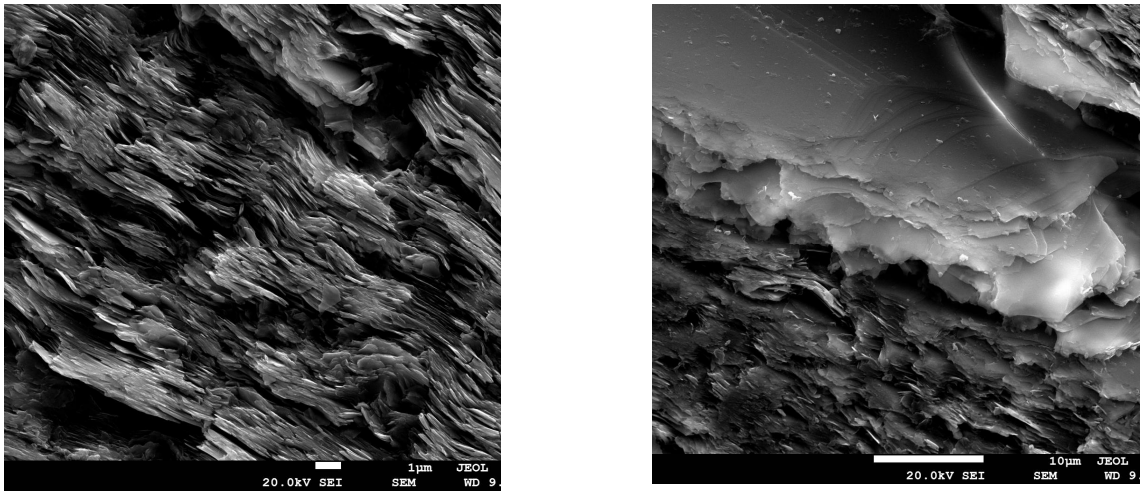

Fig 9.5. FE-SEM images of the structure of biotite in the veined gneiss cube. The roughness on the surface is due to the edges of the layered sheets and in the upper part of the right picture a basal plane can be seen.

Furthermore, it has been discovered in previous studies that of the minerals investigated in this study, the sorption of caesium is also most preferential on biotite [Muuri, E. et al., 2015]. A three site cation exchange model created by Bradbury and Baeyens has been used to explain the sorption behaviour of caesium on biotite. In low concentrations the selectivity is relatively high and constant as virtually all sorption occurs on the specific Frayed Edge Sites (FES) possessing a high affinity. As the concentration of the sorbing ion is increased, the sorption is decreased when the specific sites of the mineral become saturated. As a consequence, the sorption will occur on the non-specific and low affinity sites, Planar and Type II, sites [Bradbury, M.H. and Baeyens, 2007].

A similar model approach as with caesium was used to model the sorption of barium onto biotite. It was discovered that the model (curve) described the sorption behaviour of barium on biotite fairly well (9.4.). However, it was discovered that the model underestimates the sorption of barium for high concentrations (10^{-6} M to 10^{-3} M). A similar phenomenon has been previously reported for other metals having a charge of +II, such as Zn(II) [Tertre, E. et al., 2009]. One explanation for the phenomenon is that the

presence of high Na^+ concentration makes the study of the competition between the ions difficult. However, this has not been confirmed in this study.

9.1.5. Veined gneiss

In addition to the main minerals of the crystalline rock in the Olkiluoto and Grimsel sites, batch sorption experiments were also conducted for the main rocks of the sites. Firstly, veined gneiss from the Olkiluoto site was studied. The sorption behaviour of barium on veined gneiss followed the trend of the main minerals (Fig 9.6.). The distribution coefficients were 0.111±0.001 m^3/kg in 10^{-7} M in the Olkiluoto groundwater simulant.

The main mineral of veined gneiss is biotite (up to 50 %) and, as a consequence, the three site sorption model obtained for biotite was applied to model the experimental sorption results. It can be seen from Figure 9.6. that the model could be fit to the experimental data relatively well. The fitting parameters used in the models for biotite and veined gneiss are presented in Table 9.1. It can be seen in the table that the portion of the FES sites is very small in all investigated materials, which may be due to steric hindrance [Kodama, T. and Komarneni, S., 1998]. Ba^{2+} ions are fairly large ions whereas the interlayer sites are sterically hindered by the surrounding ions.

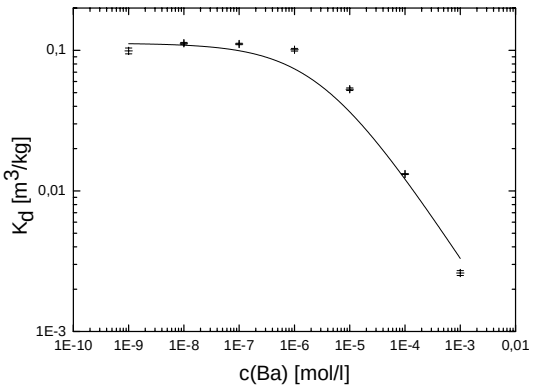

Fig 9.6. The distribution coefficients of barium as a function of barium concentration on veined gneiss in the presence of Olkiluoto groundwater simulant at pH 7.8. All data points represent the average of triplicate samples and the uncertainties are given as the standard deviation of the mean. The curve represents the modelled data.

Table 9.1. Computed selectivity coefficients and capacities for the three sites in the investigated materials acquired from the three site sorption model.

	Veined gneiss	**Biotite (Olkiluoto)**	**Biotite (Grimsel)**
Site Capacity			
– Planar	96.78 %	96.78 %	99.14 %
– Type II	2.79 %	2.64 %	0.86 %
– FES	0.43 %	0.58 %	0.1 %
log*k*(Ba)			
– Planar	3.0	3.0	2.0
– Type II	3.0	3.0	3.5
– FES	6.2	6.2	5.5

9.1.6. Pegmatite

The sorption of barium was also studied on pegmatite obtained from the Olkiluoto site (Fig 9.7.). Pegmatite is mostly consisted of large grains of quartz (15 %), plagioclase (30 %) and potassium feldspar (40 %). It was discovered in the experiments that the distribution coefficients of barium on pegmatite were approximately a magnitude smaller than those on veined gneiss with values of 0.0109±0.001 m^3/kg in 10^{-7} M (Table 9.2.) which is most probably due to the difference in the concentration of biotite in the samples.

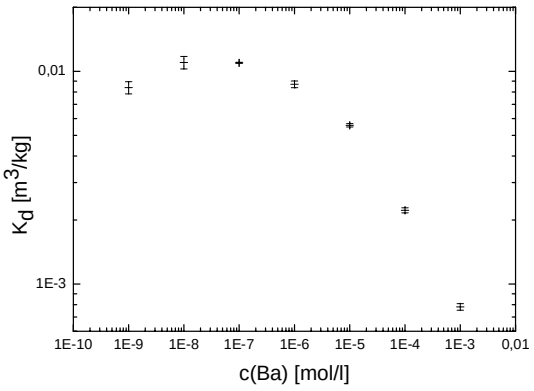

Fig 9.7. The distribution coefficients of barium on pegmatite as a function of barium concentration in the presence of Olkiluoto groundwater simulant at pH 7.7. All data points represent the average of triplicate samples and the uncertainties are given as the standard deviation of the mean.

9.1.7. Granodiorite

Lastly, the sorption behaviour of barium on granodiorite from the Grimsel site was studied (Fig 9.8.). Granodiorite is consisted of quartz (30 %), plagioclase (40%) and potassium feldspar (20 %). The distribution coefficients of barium on granodiorite were even larger than on veined gneiss with values of 0.184±0.010 m^3/kg in 10^{-7} M in the Olkiluoto groundwater simulant (Table 9.2.). The large distribution coefficients can be explained with the ionic strength of the Grimsel groundwater simulant, which is much smaller than that of the Olkiluoto groundwater simulant. As a result, there are less competing ions in the Grimsel groundwater simulant which can be explain the large distribution coefficients of barium on granodiorite compared to pegmatite, another rock containing only 5 % of biotite.

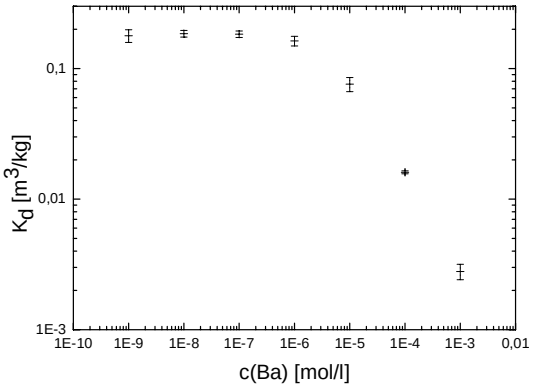

Fig 9.8. The distribution coefficients of barium on granodiorite as a function of barium concentration in the presence of Grimsel groundwater simulant at pH 8.6. All data points represent the average of triplicate samples and the uncertainties are given as the standard deviation of the mean.

It was discovered in the experiments that one of the most important factors affecting the sorption behaviour of the minerals is the specific surface area. Biotite has a large surface area, due to which barium is sorbed effectively on its surface. Furthermore, veined gneiss contains a lot of biotite (50 %), due to which barium is sorbed effectively also on its surface. The distribution coefficients were thus corrected with the specific surface areas to study the effect of specific surface area on the sorption more accurately (Table 9.2.). It was discovered that the correction reduces the differences of the distribution coefficients

of the minerals and rocks. This enforces the assumption that the specific surface area acts an important role in the distribution coefficient results.

Table 9.2. The distribution coefficients, specific surface areas and distribution coefficients corrected with the specific surface areas for all the investigated minerals and rocks.

	Distribution coefficient K_d [m^3/kg]		**Surface area SA [m^2/g]**	**K_d/SA**	
	Olkiluoto	**Grimsel**		**Olkiluoto**	**Grimsel**
Quartz	0.002	0.001	0.321	0.006	0.003
Plagioclase	0.009	0.244	0.605	0.015	0.404
Potassium feldspar	0.003	0.140	0.657	0.005	0.213
Biotite	0.084	0.286	4.566	0.018	0.063
Veined gneiss	0.111		1.480	0.075	
Pegmatite	0.011		0.342	0.032	
Granodiorite		0.184	0.330		0.557

9.2. Diffusion coefficients

It was discovered in the diffusion experiments that the tracer decrease of barium was most remarkable in granodiorite whilst the tracer decrease in veined gneiss and pegmatite was roughly similar (Fig 9.10.). This might be due to the differences of the rock structures. The granodiorite is the most permeable of the rocks and veined gneiss the least [Möri, A. et al., 2003; Ikonen, J. et al., 2015]. However, all three rock samples have similar porosities, approximately 0.5±0.2 % [Kelokaski, M. et al., 2010]. In addition, granodiorite contained only a moderate concentration of biotite in which the barium can be sorbed. Veined gneiss contained biotite copiously and it was not highly permeable. Thus the in-diffusion of barium can slow down due to the abundant sorption. In addition, pegmatite is also moderately permeable and it contains only scarcely biotite which offers sorption area for barium which might act as a slowing agent for the concentration depletion of the tracer solution.

The diffusion modelling was done to fit the experimental data acquired from the diffusion experiments as described earlier. It was discovered from the model that the diffusion coefficient of barium was largest in granodiorite ($5 \cdot 10^{-12}$ m^2/s) whilst the diffusion coefficients in veined gneiss and pegmatite were clearly lower at $8 \cdot 10^{-14}$ m^2/s. The larger diffusion coefficient in granodiorite implies the higher permeability of the rock which hastens the in-diffusion process.

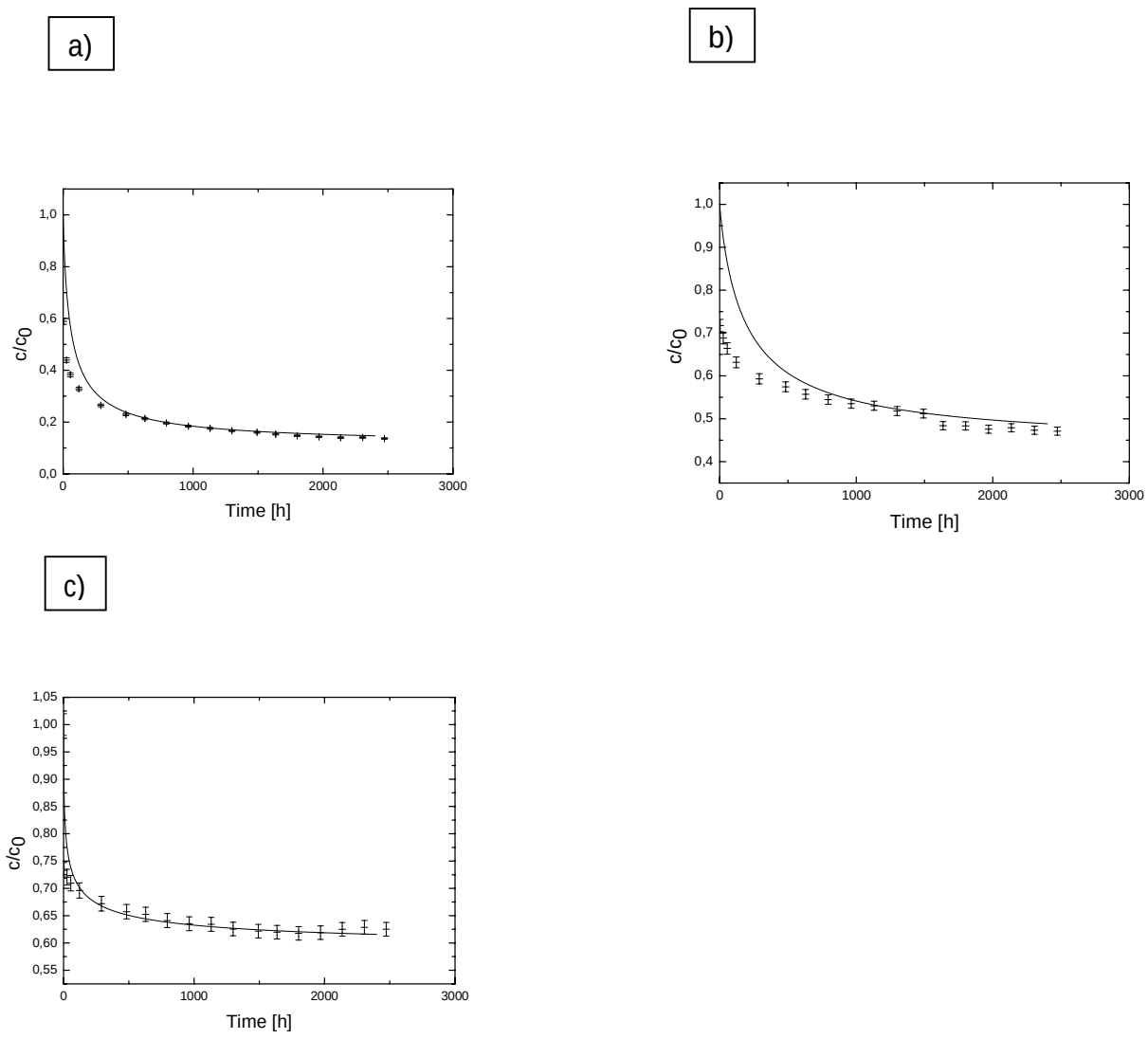

Fig 9.10. The relative tracer depletion of barium in solution and the diffusion model acquired by Comsol Multiphysics (curve) of a) granodiorite, b) veined gneiss and c) pegmatite. Each of the data points represent an average of triplicate samples and the uncertainties are given as the standard deviation of the mean.

In addition to the diffusion coefficients, also distribution coefficients were used as fitting parameters in the model. The distribution coefficient of barium acquired from the model was $0.6 \cdot 10^{-3}$ m^3/kg for granodiorite, $0.2 \cdot 10^{-3}$ m^3/kg for veined gneiss and $0.4 \cdot 10^{-3}$ m^3/kg for pegmatite. As a rule, the distribution coefficients acquired from the model were approximately three orders of magnitude smaller than the values acquired from the batch experiments. However, the distribution coefficients were also calculated from the rock cube experiments with the equation (8.1.) and the results were $1.0 \cdot 10^{-2}$ m^3/kg for granodiorite, $1.1 \cdot 10^{-3}$ m^3/kg for veined gneiss and $3.5 \cdot 10^{-4}$ m^3/kg for pegmatite, which are closer to the computed values. The great difference in the values of the batch and the cube experiments is most probably due to specific surface area. The samples used in the batch sorption experiments were milled and sieved to a grain size of < 0.3 mm. However, the rock cubes used in the diffusion experiments were intact rock. Thus, the rock cubes offer much less specific surface area for the sorption to occur. Unfortunately, the specific surface area of the rock cubes could not be determined.

Furthermore, the distribution coefficient of barium in pegmatite was smaller than the one of veined gneiss in the batch sorption experiments but the value acquired from the model was slightly larger. However, the difference was small enough to be in the limits of uncertainty. Additionally, the model did not take into account the heterogeneity of the mineralogy in the rock samples, which is evident in the autoradiogram and FE-SEM images. Finally, a larger porosity was set for pegmatite to fit the model to the experimental data after the data of large fissures was acquired from the FE-SEM (Table 9.2.). Preliminary diffusion experiments have been conducted for barium in the Grimsel test site and the unpublished results are similar to the results acquired in this study.

Table 9.2. The distribution coefficients, diffusion coefficients and porosities acquired from the Comsol Multiphysics diffusion model.

	Distribution coefficient [m^3/kg]	**Diffusion coefficient [m^2/s]**	**Porosity [%]**
Granodiorite	$0.6 \cdot 10^{-3}$	$5 \cdot 10^{-12}$	0.65
Veined gneiss	$0.2 \cdot 10^{-3}$	$8 \cdot 10^{-14}$	0.2
Pegmatite	$0.4 \cdot 10^{-3}$	$8 \cdot 10^{-14}$	4

Additionally, it can be seen from the in diffusion curves that the concentration decrease is more dramatic in the beginning of the experiment (0-500 h) after which the depletion started to moderate suggesting an approach of an equilibrium state. In addition, the rapid decrease in the first few hours of the experiment suggests a surface phenomenon, sorption, and that the mineral surfaces of rock are readily accessible for ions in the tracer solution. The depth of penetration was not studied quantitatively as all the facets of the cube were exposed to the tracer solution and one dimensional investigation of the sample was difficult. Thus, the diffusion modelling conducted with Comsol Multiphysics was only a preliminary study and the model should validated with TDD modelling.

9.3. The spatial distribution of activity in the autoradiograms

It was discovered in the autoradiograms of the rock cubes that the radioactive barium was sorbed most preferentially in the dark mica minerals of the rocks (Fig 9.11.). This has been previously discovered for caesium in numerous studies. The sheet structure of the mica leaves the cations usually in the edge of the interlayer of the structure where they can be exchanged with other ions [Fuller, A.J. et al., 2014]. On the other hand, the sorption on, for example, quartz is much smaller than on biotite as the grain size of quartz in intact rock is usually larger and the surface of quartz is mostly consisted of basal planes making the specific surface area significantly smaller than that of biotite.

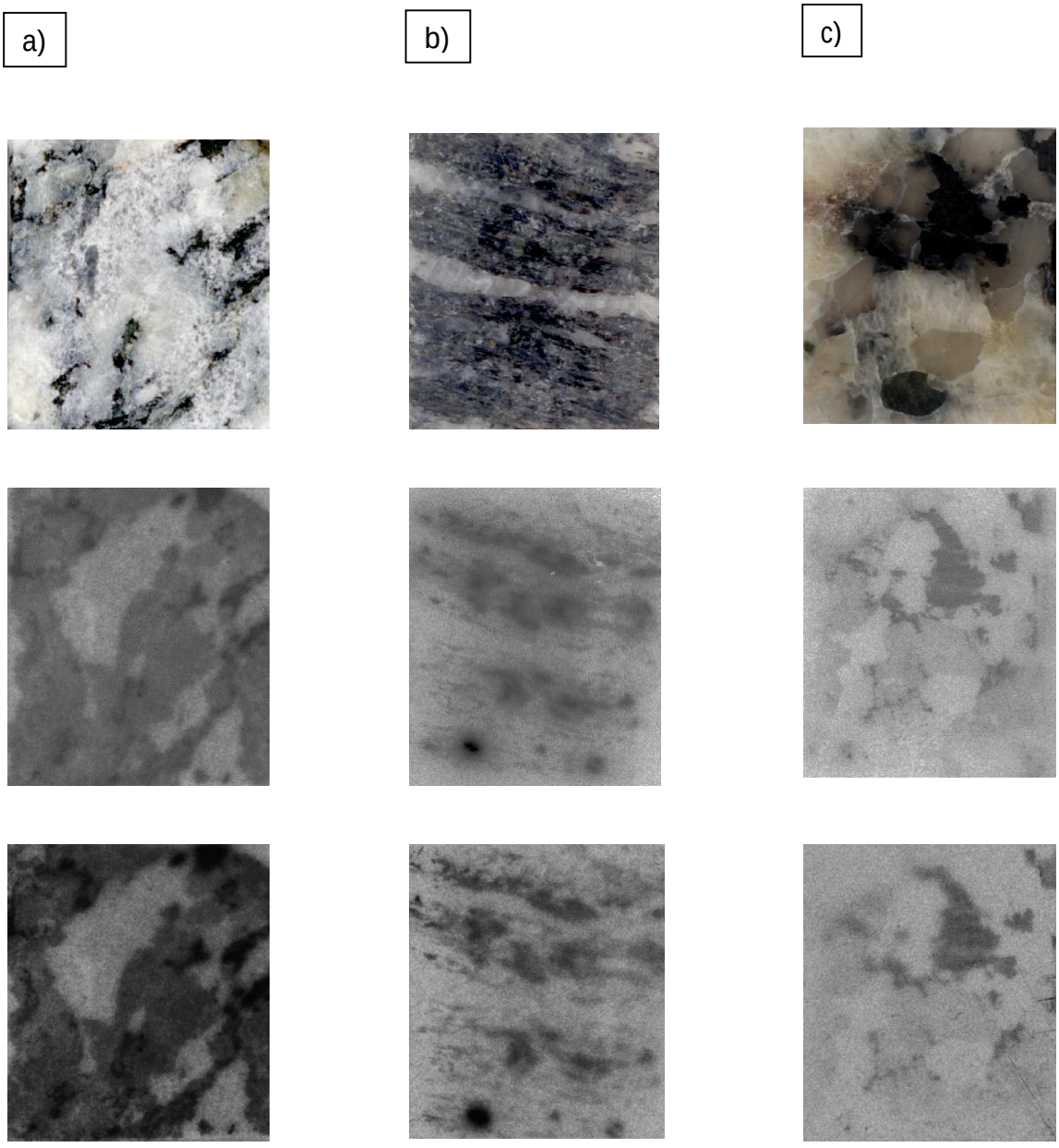

Fig 9.11. The digital images (upper), digital autoradiograms (middle) and film autoradiograms (lower) of a) granodiorite, b) veined gneiss and c) pegmatite.

It can be seen from the autoradiograms that the resolution of film autoradiography is slightly better than that of digital autoradiography. In addition, it can be seen that the some parts of the autoradiograms are slightly blurred. This is due to the samples not being in proper contact with the phosphor screen or the film, as is the case with the film autoradiography image of pegmatite where the left part of the sample has clearly not been in proper contact with the film. This may be caused by the lead sheets not being evenly distributed on the samples.

It is also evident from the autoradiograms that whereas in pegmatite and veined gneiss the barium is mostly in dark minerals, in granodiorite barium is distributed more evenly also in the light minerals. The structure of granodiorite is more brittle than pegmatite and veined gneiss and consisted of evenly distributed small grains, which adds to the specific surface of the rock. This can explain the more even distribution of radioactive barium on the surface of the granodiorite samples. The structure of the veined gneiss and pegmatite is more heterogeneous, especially pegmatite is consisted of larger grains, which makes also the spatial distribution of barium more heterogeneous.

The rock cubed were sawed to thin slices to study the penetration depth of barium in the rock cubes. However, it could only be studied qualitatively as quantitative study would have required activity standards for barium which were not accessible in this study. It was discovered in the autoradiograms prepared from the rock slices that the barium had been penetrated more deeply in pegmatite and granodiorite than in veined gneiss. Pegmatite and granodiorite contain more fissures offering diffusion routes in the structure of the rock. The fissures in veined gneiss are scarcer and less connected to each other due to the heterogeneous structure [Ikonen, J. et al., 2015]. In addition, barium is sorbed strongly on the biotite abundant in the rock slowing down the in diffusion process.

9.4. Elemental maps

To investigate the initial elemental compositions of the rocks, samples that had not been in contact with the barium tracer solution were studied. It was discovered that none of the rock types investigated contained natural barium or the amounts were so low that they could not be detected with the FE-SEM system used. Thus, when the rock cubes from the diffusion experiment were studied, it could be concluded that all the barium seen in the images was originated from the tracer solution.

The samples containing veined gneiss were studied and it was discovered that the samples contained magnesium-rich biotite abundantly and quartz and feldspars quite scarcely. The samples were polished well, which could be seen from the relatively small roughness of the surface. The sorbed barium was detectable with the FE-SEM system used. The sorbed barium could mainly be detected in the biotite veins in the rock sample, most preferably in veins where there were also a few fissures.

There was practically no calcium in the samples of veined gneiss that were studied. However, magnesium was abundant and it was detected that the barium deposits followed the locations of the magnesium deposits in the biotite, which can be seen as the light area in the backscattered electron image (Fig 9.12.). Furthermore, no sulphur or phosphorus was detected so it could be concluded that the discovered barium was detached through ion exchange and that it was not precipitated on the surface as sulphate or phosphate.

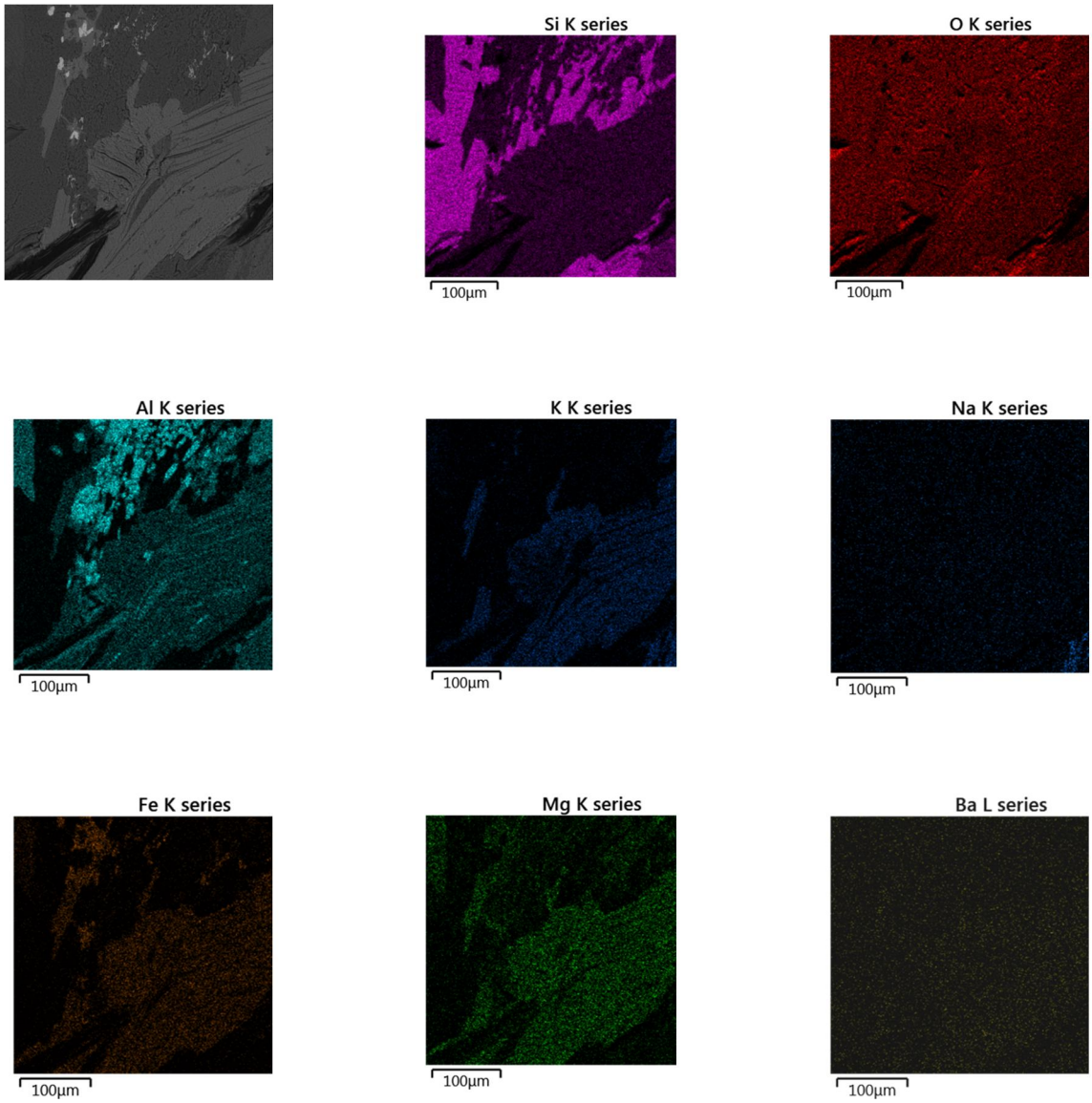

Fig 9.12. The backscattered electron image (upper left) and the elemental maps of a veined gneiss site of the rock cube.

Granodiorite samples were studied to find the sorbed barium. It was discovered that the samples contained mainly quartz and feldspars with veins rich in calcium. The barium deposits followed the calcium deposits in the sample. Additionally, no sulphur or phosphorus was discovered in the samples which reinforces that the barium seen in the SEM images is detached with ion exchange and not due to precipitation.

It was discovered in the SEM imaging that the calcium deposits were found as veins of plagioclase in between of potassium feldspar grains. It is common that potassium feldspar contains inclusions of plagioclase as veined structures as they are formed in similar conditions but different temperatures in the cooling of the rock melt [Klein, C. and Dutrow, B., 2007]. These veins following the fissures of the rock may provide preferential surface area for the sorption sites.

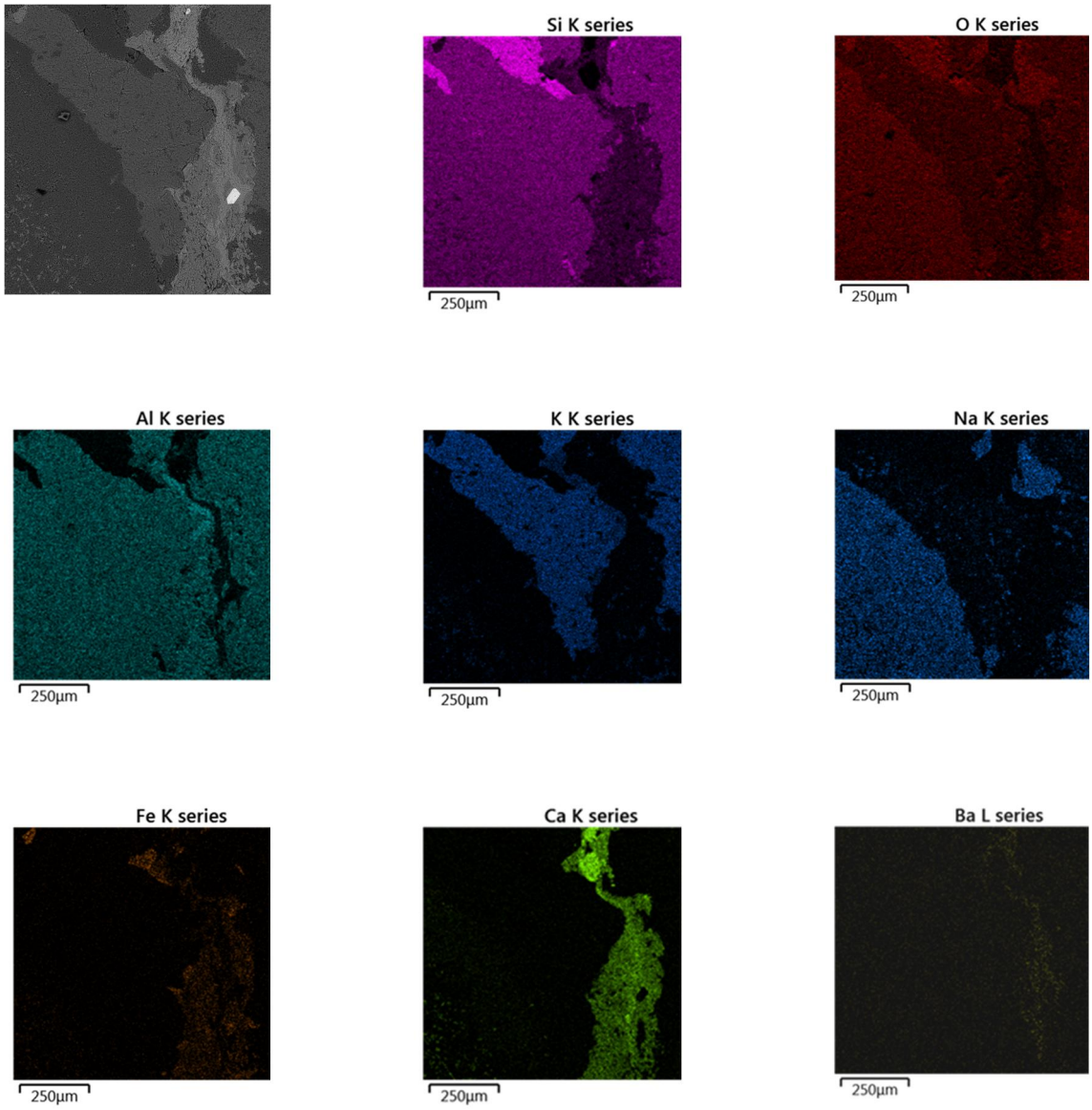

Fig 9.13. The backscattered electron image (upper left) and the elemental maps of a granodiorite site of the rock cube.

The sample of pegmatite was also studied with the FE-SEM. It was discovered in the imaging that the majority of the sample consisted of quartz, plagioclase and potassium feldspar. The barium deposits in pegmatite followed the magnesium deposits in biotite, as with veined gneiss. However, only little biotite was found in the samples and, as a consequence, barium was found scarcely (Fig 9.14.). This is in good agreement with the results from the batch sorption experiments and diffusion experiments.

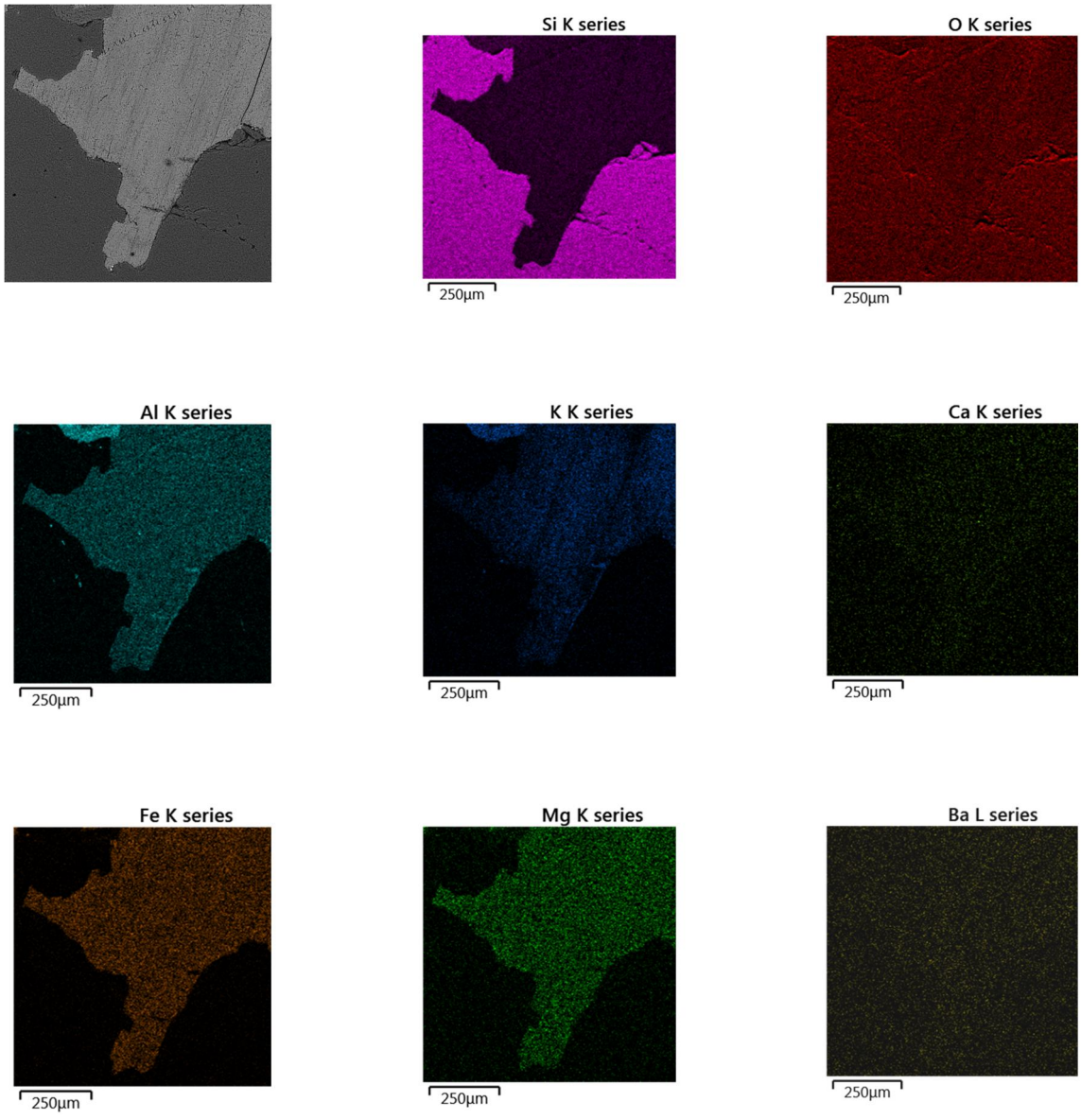

Fig 9.14. The backscattered electron image (upper left) and the elemental maps of a pegmatite site of the rock cube.

10. Conclusions and future work

10.1. Conclusions

The distribution coefficients of barium obtained from the batch experiments were largest on biotite and plagioclase. The large sorption on biotite could be explained with the edges of the layered structure providing a large surface area. The sorption of barium on quartz was found to be very small in all investigated concentrations in both groundwater simulants, which could be explained with the low ion exchange capacity of quartz. In addition, the distribution coefficients of barium on potassium feldspar were smaller than on the structurally similar plagioclase and the difference could be accounted by the stability of the structure of microcline which offers less preferential sorption sites than plagioclase.

The sorption of barium on biotite was found to behave according to the three site model validated earlier with PHREEQC for the sorption of trace metals on illitic and mica minerals. At low barium concentrations ($<10^{-6}$ M) barium was sorbed mainly on the selective FES of biotite. After the saturation of FES, barium sorbs additionally on the Type II and Planar sites which leads to the reduced selectivity at high concentrations ($>10^{-6}$ M). The three site model acquired for biotite described the sorption behaviour of barium quite successfully and can be used also in the future to interpret the sorption of barium.

The sorption behaviour of barium on crushed veined gneiss, pegmatite and granodiorite followed the sorption trend of their main minerals. It was concluded that the sorption was highest on granodiorite due to the low ionic strength of the Grimsel groundwater simulant used providing less competing ions for the sorption than in the Olkiluoto groundwater simulant. Of the rocks, the distribution coefficients were smallest in pegmatite, which is mostly consisted of large grains of quartz (15 %) and feldspars (70 %) providing less specific surface area for the sorption to occur on than biotite. The sorption of barium on veined gneiss was approximately as high as on granodiorite, which is mostly due to the large abundance of biotite (50 %).

The sorption results of the crushed rocks obtained from the laboratory experiments were systematically smaller than the sorption results obtained for the rock cubes. This is most probably due to the specific surface area, which is increased by the crushing of the rock. It has been discovered also in previous studies that the specific surface area has a significant role in trace metal sorption on mineral surfaces accounting for the large differences between the batch sorption experiments and the in-situ experiments. In addition, the distribution coefficients followed moderately the trend of the specific surface areas implying that the specific surface area of the rock is an important tool in assessing the sorption behaviour of radionuclides.

The results acquired from these experiments for barium were in good accordance with the results acquired in earlier experiments for caesium. A clear effect of the ionic strength could be seen from the batch sorption experiments. The distribution coefficients were systematically nearly a magnitude larger in Grimsel groundwater simulant than in Olkiluoto groundwater simulant which is more saline. It could thus be concluded that the cations present abundantly in the Olkiluoto groundwater simulant compete extensively with the sorption of barium. This effect must be taken into consideration in the safety assessments of the final disposal of nuclear waste.

The concentration decrease was found to be largest in granodiorite in the diffusion experiments. This can be explained with the porous structure and high permeability of granodiorite and with the extensive sorption of barium on granodiorite. The concentration decrease was smallest in pegmatite although the diffusion coefficients of pegmatite and veined gneiss were similar, due to which it could be concluded that the most important factor dominating the concentration decrease of the tracer is sorption.

Finally, it was confirmed in the autoradiograms and FE-SEM images that the sorption was most preferential in the biotite and the fissures of the rock cubes. Additionally, the sorbed barium was also found in the fissures of the rocks which can be explained with the additional surface area released by the fracturing process. Only little barium was found in the FE-SEM images due to the poor sensitivity of the method. To obtain better elemental maps, the more sensitive EPMA method could be used.

10.2. Future research

It was assumed in this study that the sorption and diffusion behaviour of radium is analogous to barium and that the results of barium can be applied to the migration assessment of radium. It is thus highly important to study the sorption and diffusion behaviour of radium in the future to better assess the use of the analogue.

The diffusion model constructed with Comsol Multiphysics should be validated in the future by an analytical mathematical solution and, in addition, with the heterogeneous time domain diffusion model. Thus, it can be assessed how well the model obtained in this study performs with the experimental data. Furthermore, a transport model using PHREEQC can also be performed to assess the validity of the diffusion model, although as a one dimensional model it can only describe a simple solution of the model. The diffusion experiments in the studied rock types should also be studied with different radionuclides. Additionally, in diffusion of radionuclides needs be studied as a function of diffusion distance from the surface.

REFERENCES

Boving, T. and Grathwohl, T. Tracer diffusion coefficients in sedimentary rocks: correlation to porosity and hydraulic conductivity. Journal of Contaminant Hydrology. Volume 53, Issues 1–2, 2001, Pages 85–100

Boyd, G.A. Autoradiography in Biology and Medicine. Academic Press Inc, New York. 1955.

Bradbury, M.H. and Baeyens, B. A generalized sorption model for the concentration dependent uptake of caesium by argillaceous rocks. Journal of Contaminant Hydrology. 42(2000) 141-163.

Brundle, C.R., Evans, C.A. Jr., Wilson, S. ENCYCLOPEDIA OF MATERIALS CHARACTERIZATION: Surfaces, Interfaces, Thin Films. Manning Publications Co. 1992.

Catalette, H., Dumonceau, J. and Ollat, P. Sorption of cesium, barium and europium on magnetite. Journal of Contaminant Hydrology. Vol 35 (1-3) 1998. 151-159.

Celebi, O., Kilikli, A. and Erten, H.N. Sorption of radioactive cesium and barium ions onto solid humic acid. Journal of Hazardous Materials. 168 (2009) 695-703

Cole, D.R. Leaching and diffusion in rocks and their weathering products: Theory and application of adsorption and ion exchange reaction kinetics to in situ leaching of ores. Theoprastus publications S.A. 1983.

Comsol. Comsol multiphysics user's guide. Version 4.3. 2012. Available http://nf.nci.org.au/facilities/software/COMSOL/4.3/doc/pdf/mph/COMSOLMultiphysicsUsersGuide.pdf

Cussler, E.L. Diffusion: Mass Transfer in Fluid Systems. Third edition. 2009. Cambridge university press.

Fernandes, M.M. and Baeyens, B. Radionuclide retention at mineral-water interfaces in the natural environment. In Poinssot, C. and Geckeis, H. Radionuclide Behaviour in the Natural Environment, 1st Edition. Science, Implications and Lessons for the Nuclear industry. Woodhead Publishing, USA. 2012.

Ferrell, R.E., Aagaard, P., Forsman, J., Greenwood, L. and Zheng, Z. Application of a geochemical transport model to predict heavy metal retention (Pb) by clay liners. Applied Clay Science 21(2002) 59-66.

Fichet, P. Bresson, F., Leskinen, A., Goutelard, F., Ikonen, J. and Siitari-Kauppi, M. Tritium analysis in building dismantling process using digital autoradiography. J Radioanal Nucl Chem (2012) 291:869–875.

Friel, J.J. X-ray and image analysis in electron microscopy. Second edition. Princeton gamma-tech. 2003.

Fuller, A.J., Shaw, S., Peacock, C.L., Trivedi, D., Small, J.S., Abrahamsen, L.G. and Burke, I.T. Ionic strenght and pH dependent multi-site sorption of Cs onto a micaceous aquifer sediment. Appl. Geochem. 2014. 40(1). 32-42

Goldberg, S., Criscenti, L.J., Turner, D.R., Davis, J.A. and Cantrell, K.J. Adsorption–Desorption Processes in Subsurface Reactive Transport Modeling. Vadose Zone Journal. 6. 407-435

Goldstein, J.I., Newbury, D.E., Echlin, P., Joy, D.C., Roming, A.D., Lyman, C.E., Fiori, C. and Lifshin, E. Scanning Electron Microscopy and X-Ray Microanalysis. A text for biologists, materials scientists and geologists. Plenum Press, New York. 2012.

Greenwood, N.N. and Earnshaw, A. Chemistry of the Elements. Oxford: Pergamon. 1997. p. 107-113

Hakanen, M., Ervanne, H. and Puukko, E. Safety Case for the Disposal of Spent Nuclear Fuel at Olkiluoto: Radionuclide Migration Parameters for the Geosphere. Posiva Oy. 2012-41

Hayes, K.F., Redden, G., Ela, W. and Leckie J.O. Surface Complexation Models: An Evaluation of Model Parameter Estimation Using FITEQL and Oxide Mineral Titration Data. Journal of Colloid and Interface Science, Vol. 142, No. 2, 1991

Hayes, P.L., Malin, J.N., Konek, C.T. and Geiger, F.M. Interaction of Nitrate, Barium, Strontium and Cadmium Ions with Fused Quartz/Water Interfaces Studied by Second Harmonic Generation. J. Phys. Chem. A 2008. 112. 660-668.

Hedin, A. et. al. Long-term Safety for KBS-3 Repositories at Forsmark and Laxemar – a first evaluation. SKB TR-06-09, Svensk Kärnbränslehantering AB. 2006.

Hellmuth, K-H., Siitari-Kauppi, M. and Lindberg, A. Study of porosity and migration pathways in crystalline rock by impregnation with ^{14}C-polymethylmetacrylate. J. Cont. Hydl. 13(1-4) 403-418. 1993.

Hoehn, E., Eikenberg, J., Fierzb, T., Drostc, W. and Reichlmayrc, E. The Grimsel Migration Experiment: field injection-withdrawal experiments in fractured rock with sorbing tracers. J. Contam. Hydrol. 1998. 34(1-2). 85-106.

Hu, Q. and Möri, A. Radionuclide transport in fractured granite interface zones. Physics and Chemistry of the Earth, Parts A/B/C Volume 33, Issues 14–16, 2008, Pages 1042–1049.

Huitti, T. Hakanen, M. and Lindberg, A. Sorption of cesium on Olkiluoto mica gneiss,

granodiorite and granite. POSIVA 98-11. 1998.

Ikonen, J., Sammaljärvi, J., Siitari-Kauppi, M., Voutilainen, M., Lindberg, A., Kuva, J. and Timonen, J. Investigation of rock matrix retention properties supporting laboratory

studies I: Mineralogy, porosity and pore structure. Working report POSIVA 2014-68. 2015.

Klemola, S. Säteilyn ilmaisimet. In Ikäheimonen, T. Säteily ja sen havaitseminen. Radiation and Nuclear Safety Authority Finland. 2002. 122-126.

Jokelainen, J., Meski, T., Lindberg, A., Soler, J.M., Siitari-Kauppi, M., Martin, A. and Eikenberg, J. The determination of ^{134}Cs and ^{22}Na diffusion profiles in granodiorite using gamma spectroscopy. J. Radioanal. Nucl. Chem. 2012.

Juntunen, P., Ruutu, A. and Suksi, J. Determination of ^{226}Ra from rock samples using LSC. Proceedings of the International Conference on Advances in Liquid Scintillation Spectrometry. Karlsruhe, Germany. May 7-11. p. 299-302.

Klein, C. and Dutrow, B. Manual of mineral science. Wiley. 2007. 539-544.

Knoll, G.F. Radiation Detection and Measurement. John Wiley & Sons, Inc. 2010. 235-730.

Knol, R.J.J., Bruin, K., Jong, J., Berthe, L.F., Eck-Smith and Booij, J. In vitro and ex vivo storage phosphor imaging of short-living radioisotopes. Journal of Neuroscience Methods. 168(2008) 341-357.

Kodama, T. and Komarneni, S. Na-4-mica: Cd2+, Ni2+, Co2+, Mn2+ and Zn2+ ion exchange. J. Mater. Chem., 1999, 9, 533–539.

Kuva, J., Myllys, M., Timonen, J., Kelokaski, M., Ikonen, J., Siitari–Kauppi, M., Lindberg, A. and Aaltonen, I. Microstructure, Porosity and Mineralogy Around Fractures in Olkiluoto Bedrock. Posiva Oy. 2012. POSIVA 2012-02.

Kyllönen, J., Hakanen, M., Lindberg, A., Harjula, R., Vehkamäki, M. and Lehto, J. Modeling of cesium sorption on biotite using cation exchange selectivity coefficients. Radiochimica Acta. 2014. 102(10) 919-929.

Kämäräinen, E., Haaparanta, M., Siitari-Kauppi, M., Koivula, T., Lipponen, T. and Solin, O. Analysis of ^{18}F-labelled synthesis products on TLC plates: Comparison of radioactivity scanning, film autoradiography and a phoshoimaging technique. Applied radiation and isotopes. 64 (2006) 1043-1047.

Kärki, A. and Paulamäki, S. Petrology of Olkiluoto. POSIVA 2006-02

Labarre, P., Papon, J., Moreau, M-F, Madelmont, J-C and Veyre, A. A new quantitative method to evaluate the biodistribution of a radiolabelled tracer for melanoma using whole-body cryosectioning and a gaseous detector: comparison with conventional tissue combustion technology. European Journal of Nuclear medicine. Vol 25. 2. 1998.

Lehto, J. and Hou, X. Chemistry and analysis of radionuclides: laboratory techniques and methodology. Wiley-VCH. Weinham, Germany. 2011.

Lyman, C.E., Newbury, D.E., Goldstein, J.I., Williams, D.B., Romig, A.D., Armstrong, J.T., Echlin, P., Fiori, C.E., Joy, D.C., Lifsin, E. and Peters, K-R. Scanning electron microscopy, X-ray microanalysis and analytical electron microscopy. A laboratory workbook.Plenum Press, New York. 1990.

McKinley, J.P., Zachara, J.M., Healds, S.M., Dohnalkova, A., Neville, M.G. and Sutton, S. Microscale Distribution of Cesium Sorbed to Biotite and Muscovite. Environ. Sci. Techol. 38, 1017(2004).

Miller, B. and Marcos N. Process report –FEPs and scenarios for a spent fuel repository at Olkiluoto. Posiva Oy. 2007. Posiva report. 2014.

Millington, R.J., and J.M. Quirk. 1961. Permeability of porous solids. Petersen, L.W., D.E. Rolston, P. Moldrup, and T. Yamaguchi. 1994. Trans. Faraday Soc. 57:1200–1207.

Molinero, J. and Samper, J. Large-scale modeling of reactive solute transport in fracture zones of granitic bedrocks. Journal of Contaminant Hydrology. 82. 2006. 293-318

Moreno, L., Crawford, J. and Neretnieks, I. Modelling radionuclide transport for time varying flow in a channel network. Journal of Contaminant Hydrology. 86 (2996) 215-238.

Muuri, E., Ikonen, J., Matara-aho, M., Lindberg, A., Holgersson, S., Voutilainen, M., Siitari-Kauppi, M. and Martin A. Behavior of Cs in Grimsel granodiorite Part I: Sorption on main minerals and crushed rock. To be submitted.

Möri, A., Alexander, W.R., Geckeis, H., Hauser, W., Schäfer, T., Eikenberg, J. and Fiertz, T. The colloid and radionuclide retardation experiment at the Grimsel test site: influence of bentonite colloids on radionuclide migration in a fractured rock. Colloids Surf., A. 2003. 217(1-3). 33-47.

Möri, A., Mazurek, M., Adler, M., Schild, M., Siegesmund, S., Vollbrecht, A., Ota, K., Ando, T., Alexander, W.R., Smith, P.A., Haag, P. and Bühler, C. Grimsel Test Site Investigation Phase IV (1994-1996) The Nagra-JNC in situ study of safety relevant radionuclide retardation in fractured crystalline rock. IV: The in situ study of matrix porosity in the vicinity of a water conducting fracture. Technical report 00-08. 2003.

Mäder, U.K., Fierz, T., Frieg, B., Eikenberg, J., Rüthi, M., Albinsson, Y., Möri, A., Ekberg, S. and Stille, P. Interaction of hyperalkaline fluid with fractured rock: Field and laboratory experiments of the HPF project (Grimsel test site, Switzerland). J. Geochem. Explor. 2006. 90(1-2). 68-94.

Nagata, T., and Fukushi, K. Prediction of iodate adsorption and surface speciation on oxides by surface complexation modelling. Geochimica et Cosmochimica Acta. /4(2010) 6000-6013.

National Nuclear Data Center, information extracted from the NuDat 2 database, http://www.nndc.bnl.gov/nudat2/

NEA. Spent Nuclear Fuel Assay Data for Isotopic Validation. Nuclear Science NEA/NSC/WPNCS/DOC(2011)5 June 2011.

Neall, F., Pastina, B., Smith, P., Gribi, P., Snellman, M. and Johnson, L. Safety Assessment for a KBS-3H Spent Nuclear Fuel Repository at Olkiluoto: Complementary Evaluations of Safety Report. Posiva Oy. POSIVA 2007-10

O'Day, P.A. Molecular environmental geochemistry. Rev. Geophys. 1999. 37, 249-274.

Parkhurst, D.L. and Appelo, C.A.J. User's guide to PHREEQC (version 2) – A computer program for speciation, batch-reaction, one-dimensional transport and inverse geochemical calculations. Water-Resources Investigations Report 99-4259. Denver, Colorado. 1999.

Peterson, J., Macdonell, M., Haroun, L. and Monette, F. Radiological and Chemical Fact Sheets to Support Health Risk Analyses for Contaminated Areas. Argonne National Laboratory Environmental Science Division. 2007. Available http://www.remm.nlm.gov/ANL_ContaminantFactSheets_All_070418.pdf

Pitkänen, P., Snellman, M. & Vuorinen, U. 1996. On the origin and chemical evolution of groundwater at the Olkiluoto site. Posiva Oy, Eurajoki, Finland. Report POSIVA-96-04, 41 p.

Posiva Oy. Olkiluoto Site Description 2008 Part 2. POSIVA 2009-01.

Posiva Oy. Safety Case for the Disposal of Spent Nuclear Fuel at Olkiluoto – Synthesis 2012. POSIVA Oy. 2012-12.

Posiva Oy. Safety Case for the Disposal of Spent Nuclear Fuel at Olkiluoto – Models and data for the repository system 2012. POSIVA Oy, 2013-01.

Sajih, M., Bryan N.D., Livens, F.R., Vaughan, D.J., Descostes, M., Phrommavanh, V., Nos, J. And Morris, K. Adsorption of radium and barium on goethite and ferrihydrite: A kinetic and surface complexation modelling study. Geochimica et Cosmochimica Acta Volume 146, 2014, Pages 150–163

Sardini, P., Caner, L., Mossler, P., Mazurier, A., Hellmuth, K-H., Graham, G.C., Rossi, A.M. and Siitari-Kauppi, M. Calibration of digital autoradiograph technique for quantifying rock porosity using ^{14}C-PMMA method. J Radioanal Nucl Chem. 2015. 303. 11-23.

Schatz, T., Kanerva, N. Martikainen, J., Sane, P. Olin, M. and Seppälä, A. Buffer Erosion in Dilute Groundwater. POSIVA 2012-44. 2013.

Schmidt, K.C. and Smith, C.B. Resolution, sensitivity and precision with autoradiography and small animal positron emission tomography: implications for functional brain imaging in animal research. Nuclear Medicine and Biology. Vol 32 (2005) 719-725.

Shahwan, T. and Erten, H.N. Temperature effects in barium sorption on natural kaolinite and chlorite-illite clays. J. Radioanal. Nucl. Chem. 260. 2004. 43-48.

Shannon, R.D. Revised effective ionic radii and systematic studies of interatomic distances in halides and chalcogenides. Acta Cryst. 1976. A32(1). 751-767

Sheha, R.R. and Metwally, E. Equilibrium isotherm modelling of cesium adsorption onto magnetic materials. Journal of Hazardous Materials. 143 (2007) 354-361.

Siitari-Kauppi, M. Development of ^{14}C-polymethylmetacrylate method for the characterisation of low porosity media: Application to rocks in geological barriers of nuclear waste storage. PhD thesis, University of Helsinki, 2002. Report Series in Radiochemistry 17.

Siitari-Kauppi, M.K., Hölttä, P., Pinnioja, S. and Lindberg, A. Cesium sorption on tonalite and mica gneiss. Mater. Res. Soc. Symp. Proc. 1999. 556(1). 1099-1106.

Smith, P.A., Alexander, W.R., Kickmaier, W., Ota., K., Frieg, B. and McKinley, I.G. Development and testing of radionuclide transport models for fractured rock: examples from the Nagra/JNC Radionuclide Migration Programme in the Grimsel Test Site, Switzerland. Journal of Contaminant Hydrology. 47 (2001) 335-348.

Soler, J.M., Landa, J., Havlova, V., Tachi, Y., Ebina, T., Sardini, P., Siitari-Kauppi, M., Eikenberg, J. and Martin, A.J. Comparative modeling of an in situ diffusion experiment in granite at the Grimsel Test Site. Journal of Contaminant Hydrology. 179 (2015) 89-101.

Stegena, L. Leaching and diffusion in rocks and their weathering products. Leaching in rocks: Some physical principles. Theoprastus publications S.A. 1983.

Stewart, B.A. Advances in Soil Science. Volume 16. Springer-Verlag New York Inc. 1991.

Stumm, W. and Morgan, J.J. Aquatic chemistry: Chemical equilibria and rates in natural waters. John Wiley & Sons, Inc. 1996. 521-575.

Stumm, W. Chemistry of the solid-water interface: Processes at the mineral-water and particle-water interface in natural systems. John Wiley & Sons, Inc., New York.

Sugiyama, S., Matsumoto, H., Hayashi, H. and Moffat, J.B. Sorption and ion-exchange properties of barium hydroxyapatite with divalent cations. Colloids and Surfaces A: Physicochemical and Engineering Aspects. 169, 1–3, 2000, 17–26

Söderlund, M., Lusa, M., Virtanen, S., Välimaa, I., Hakanen, M., Lehto, J. & Lahdenperä, A-M. Distribution Coefficients of Caesium, Chlorine, Iodine, Niobium, Selenium and Technetium on Olkiluoto Soils. 2014 Posiva. Posiva Working Report, vol 2013, nro 68.

Tachi, Y., Ebina, T., Takeda, C., Saito, T., Takahashi, H., Ohuchi, Y. and Martin, A. Matrix diffusion and sorption of Cs^+, Na^+, I^- and HTO in granodiorite: Laboratory-scale results and their extrapolation to the in situ condition. Journal of Contaminant Hydrology 179 (2015) 10–24.

Tertre, E., Beaucaire, C., Coreau, N. and Juery, A. Modelling Zn(II) sorption onto clayey sediments using a multi-site ion-exchange model. Applied Geochemistry. 24(2009) 1852-1861.

Upham, L.V. and Englert, D.F. Handbook of radioactivity analysis. Elsevier Science. 2003. 1063-1127.

Wallace, S.H. Shaw, S., Morris, K., Small, J.S., Fuller, A.J. and Burke, I.T. Effect of groundwater pH and ionic strength on strontium sorption in aquifer sediments: Implications for ^{90}Sr mobility at contaminated nuclear sites. Applied Geochemistry. Vol 27. Issue 8. 2012. 1482–1491

Widestrand, H., Andersson, P., Byegård, J., Skarnemark, G., Skålberg, M. and Wass, E. In Situ Migration Experiments at Äspö Hard Rock Laboratory, Sweden: Results of Radioactive Tracer Migration Studies in a Single Fracture. Journal of radioanalytical and nuclear chemistry. Vol 250, no 3 (2004) 501-517.

Yonekura, Y., Brill, A.B., Som, P., Bennett, G.W. and Fand, I. Quantitative Autoradiography with Radiopharmaceuticals, Part 1: Digital Film Analysis System by Videodensitometry: Concise Communication. J Nucl Med. 24. 1983. 231-237.

Öhberg, A. and Rouhiainen, P. Posiva groundwater flow measuring techniques. Posiva Oy. 2000. 2000-12.